國 立 交 通 大 學
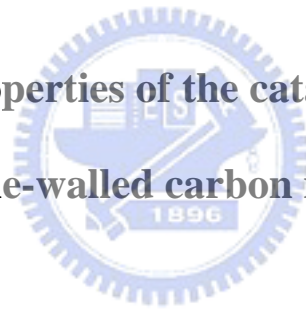
材料科學與工程研究所

碩士論文

觸媒前趨物輔助合成單壁奈米碳管
之製程及其性質

Processes and properties of the catalyst precursor-assisted

single-walled carbon nanotubes

研　究　生　：　洪　蔡　豪

指　導　教　授　：　郭　正　次　博士

中華民國九十五年七月

National Chiao Tung University

Processes and properties of the catalyst precursor -assisted single-walled carbon nanotubes

A Thesis
Submitted to Institute of Materials Science and Engineering
College of Engineering
National Chiao Tung University
In Partial
Fulfillment of the Requirements
For the Degree of Master of Science
In
Materials Science and Engineering

Student :   Tasi-Hau Hang

Advisor :   Cheng-Tzu Kuo

July 2006
Hsinchu, Taiwan, Republic of China

觸媒前趨物輔助合成單壁奈米碳管
之製程及其性質

研究生：洪蔡豪 　　　　　　　　　　　　指導教授：郭正次 教授

國立交通大學材料科學與工程研究所

摘要

為了探討觸媒前趨物，前處理方法與基材再成長對於成長單壁奈米碳管製程之影響，本研究在矽基材上鍍上$CoCrPtO_x$與$CoCrO_x$為觸媒前趨物，在氫氣與甲烷氣氛下以微波電漿輔助化學氣相沈積法(MPCVD)成長單壁奈米碳管。製程首先濺鍍緩衝層及觸媒前趨物在矽基材上。接著使用氫電漿前處理(在MPCVD系統中)或局部雷射加熱前處理(在DVD動態測試機中)使觸媒變成均勻分佈的奈米觸媒顆粒，然後在MPCVD系統中沈積碳奈米結構。前處理後的奈米觸媒顆粒與沈積後的碳奈米結構使用掃描電子顯微技術(SEM)、穿透電子顯微技術(HRTEM)、拉曼光譜技術(Raman spectroscopy)、光電子能譜儀(XPS)、熱重分析儀(TGA)以及場發射J-E測量法加以分析探討。從本研究的結果可獲得下列結論。

使用$CoCrPtO_x$觸媒前趨物並配合氫電漿前處理可基底成長出準直的單壁奈米碳管。其直徑為2~3奈米，長度為40微米。觸媒前趨物的爆炸式化學還原反應有效的使奈米觸媒顆粒變小。其機制為PtO_2的高能量還原反應使觸

I

媒前趨物薄膜爆散成奈米觸媒顆粒，而Cr_2O_3則有效的阻止奈米觸媒顆粒的聚集。

將成長後的單壁奈米碳管使用超音波震盪取下後，其矽基材可以再一次的使用來成長單壁奈米碳管。此矽基材再一次經過氫電漿前處理與化學沈積後，成長出的單壁奈米碳管之形貌與性質幾乎與第一次成長出單壁奈米碳管的完全相同，具有高品質高密度。此製程提供一個量產單壁奈米碳管的方法。

若我們使用局部雷射加溫前處理來幫助觸媒前驅物爆散為奈米觸媒顆粒，可以降低我們整體製程的溫度，並且在373^{o}C的低溫下成長出單壁奈米碳管。相對於氫電漿前處理，局部雷射加熱只是局部的單點加熱使PtO_2還原反應進行，讓觸媒爆散成奈米顆粒，整個矽基材並沒有經過高溫的處理，提供了一個在低溫下觸媒前處理與成長單壁奈米碳管的方法。

關於成長出的準直單壁奈米碳管的性質，場發射分析指出其起始電壓為 4.6 V/μm (在電流密度 0.01 mA/cm^2 時)而電流密度為 6 mA/cm^2 (在 7.2 V/μm 的電壓時)。拉曼分析結果顯示其 I_G/I_D 比高達 43。而熱重分析顯示其在空氣中的抗氧化溫度高達 586°C～691°C，此結果與雷射法成長出並且純化過的單壁奈米碳管相似。

Processes and properties the catalyst precursor-assisted single-walled carbon nanotubes

Graduated Student : Tsai-Hau Hong   **Advisor : Cheng-Tzu Kuo**

Institute of Materials Science and Engineering
National Chiao Tung University

Abstract

To examine effects of catalyst precursors, pretreatment methods and substrate recycling on the single-walled carbon nanotubes (SWNTs) formations, the processes were developed to synthesize various carbon nanostructures on Si wafer by the microwave plasma chemical vapor deposition (MPCVD) with CH_4 and H_2 as source gases, with $CoCrPtO_x$ and $CoCrO_x$ as catalyst precursors. The processes include; First, the buffer layer (AlON) and then catalyst precursors or catalysts (Co) were deposited on Si wafer by sputtering. The coated substrates were followed by H-plasma (in MPCVD system) or scanning local laser heating (in air by DVD dynamic tester) pretreatments to produce the well-distributed catalyst nanoparticles before nanostructures deposition by MPCVD method. The microstructures at each processing step and the as-deposited nanostructures and their properties were characterized by FE-SEM, TEM, HRTEM, Raman spectroscopy, XPS, TGA and I-V measurements. From

the experimental results, the following conclusions can be drawn.

The results indicate that the well-aligned and base-growth SWNTs can be synthesized by using $CoCrPtO_x$ as catalyst precursor under H-plasma pretreatment. The as-deposited SWNTs are about ~ 2.6 nm in diameter and 40 μm in length. The function of the catalyst precursor is essentially to promote miniaturization of the sizes of the catalyst nanoparticles down to about ~ 2.4 nm in diameter due to explosive chemical reactions during pretreatment process. This mechanism is based on the explosion associated with the reduction of PtO_x in the $CoCrPtO_x$ film, and Cr_2O_3 is employed to inhibit the agglomeration of nanoparticles during pretreatment and the initial stage of nanostructure deposition.

Effect of substrate recycling process was studied by removing the as-deposited nanostructures from the substrates, and the substrates were then pretreated in H-plasma to reactivate the catalyst particles on the substrate. The well-aligned SWNTs can be obtained by substrate recycling for several times. In other words, the process gives the advantage to synthesize SWNTs in mass production by cycling the catalyst-coated substrates like a template.

Regarding to the effect of the precursor-coated substrate pretreatment methods, the results show that the scanning local laser heating method gives rise to lower deposition temperatures (~ 373°C) for SWNTs formation. By

comparing with the traditional H-plasma pretreatment method, it has advantages of promoting the miniaturization of the catalyst particles at local area without high temperature heating on the whole substrate.

About properties of the well-aligned SWNTs, field emission properties indicate a turn on voltage of 4.6 V/μm (for current density 0.01 mA/cm^2) and the current density of 6 mA/cm^2 (for field strength 7.2 V/μm). The Raman spectra display the I_G/I_D ratio of the synthesized SWNTs can be reached to a value of ~ 43. The results of TGA analysis in air show that the as-deposited SWNTs can resist oxidation up to 586°C ~ 691°C, which are much higher than the reported temperatures (~ 350°C) in the literature, and are comparable with that for the purified SWNTs synthesized by a laser-oven method.

Acknowledgements

Contents

List of symbols

AES	Auger electron spectra
AFM	Atomic force microscopy
BSE	Backscattered electron
α	Effective emission area
β	Field enhancement factor
c	Speed of light
C_h	Chiral vector
CNTs	Carbon nanotubes
CRT	Cathode-ray tube
CVD	Chemical vapor deposition
DWNT	Double-walled carbon nanotubes
E	Electron field
ECRCVD	Electron cyclotron resonance chemical vapor deposition
ED	Electron diffraction
EDX	Energy-Dispersive X-Ray
FED	Field emission display
FE-SEM	Field emission scanning electron microscopy
FET	Field effect transistor
FIB	Focused ion beam
FN	Fowler-Nordheim
h	Planck constant
θ	Chiral angle
HRTEM	High resolution transmission electron microscopy
I	Field emission current
J	Field emission current density
LCD	Liquid crystal display
MWNTs	Multi-walled carbon nanotubes
MPCVD	Microwave plasma chemical vapor deposition
NIP	Nano-indentation probe
PDP	Plasma display panel
PVD	Physical vapor deposition
RBM	Radial breathe mode
RF	Radio frequency

SE	Secondary electron
SEM	Scanning electron microscopy
STM	Scanning tunneling microscope
SWNTs	Single-walled carbon nanotubes
TEM	Transmission electron microscopy
TGA	Thermal gravimetric analysis
V	Voltage
XPS	X-ray photoelectron spectroscopy
ϕ	Work function

Table captions

Figure captions

in the (f) 1-nm-thick catalyst precursor with buffer layer

Chapter I
Introduction

1.1 Introduction to single-walled carbon nanotubes

CNTs are one dimension nanostructure of carbon bonded mainly by sp^2 bond and crooked by sp^3 bonds with hollow and cylindrical construction. We can simply image that it is a graphene sheet [Fig. 1.1(a)] shaped like a roll in nano-scale [Fig. 1.1(b)]. The single-walled CNTs (SWNTs) and multi-walled CNTs (MWNTs) are defined whether the number of the rolled graphene layers is one or more. It is well known that the CNTs have extremely high aspect ratio just because the diameters of CNTs only from 1-2 nm to 8-90 nm, but the length of a tube could be from several nanometers to several micrometers.

graphite

(10,10) tube

(a)   (b)
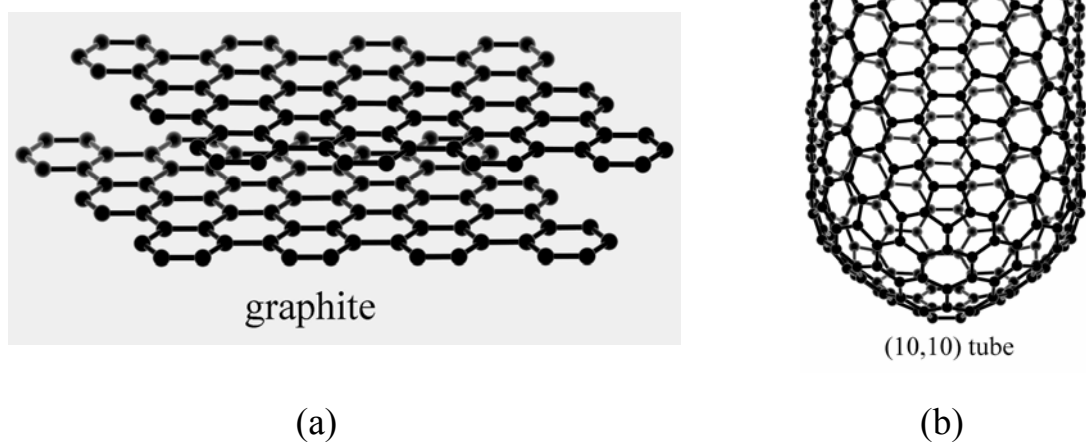
Fig. 1.1 (a) Graphite sheet (b) formed CNT rolled by the graphite sheet

[Dresselhaus-1996-p756]
.

SWNTs have attracted considerable attention in recent years. Various methods have been used for synthesizing SWNTs, e.g. arc discharge [Saito-1995-33], laser ablation [Guo-1995-49] and chemical vapor deposition (CVD) [Lee-2001-245], where the CVD methods are the most effective way to synthesize SWNTs. The SWNTs with random distribution can be easily synthesized. [Delzeit-2001-368] However, the actual growth mechanisms of SWNTs are still a controversy question.

Due to many unique properties of SWNTs, such as high aspect ratio, small radius of curvature, extraordinary mechanical strength and chemical stability, undoubtedly, SWNTs are being developed for many applications like field emission display (FED) [Sander-1998-49], biology technology [Dai-1996-147], fuel cell [Liu-1999-1127], etc.

1.2 Motivation of this research

SWNTs have recently been considered to be a promising candidate material for use in field emitters, nano-electronic devices (such as single electron transistors) [Collins-2001-706] [Bachtold-2001-1317], and others. In such applications, one of the key issues is to effectively manipulate the nanostructures at lower deposition temperatures in order to be compatible with the IC processes. Recently, low temperature processes to synthesize the catalyst-assisted SWNTs by CVD methods have been widely studied [Qin-1998-3437] [Kurt-2001-1723] [Tsai-2001-NCTU].

However, most of these deposited SWNTs show morphologies in randomly entangled fashions [Delzeit-2001-368]. The methods to grow the well-aligned SWNTs on the desired locations are not quite successful so far.

The treatment of the catalyst to minimize the catalyst particle sizes before CNTs growth represents another technological challenge in SWNTs growth. Physical vapor deposition (PVD) is the most popular approach for depositing catalytic materials, because it is highly compatible with the IC process. The catalyst films are typically treated with H-plasma to become well-distributed nano-particles, and CNT are subsequently grown from these pre-treated catalystic nano-particles. However, the agglomeration of nano-particles is unavoidable during the heating process, which does not particularly favor the fabrication of SWNTs. One way to minimize the catalyst particle size is to use the ultra-thin catalytic film, but the agglomeration effect during H-plasma pretreatment makes it difficultly to form SWNTs[Delzeit-2001-368]. Although Zhong et al. [Zhong-2005-1558] recently reported using $Al_2O_3/Fe/Al_2O_3$ with a sandwich-like structure to fabricate vertically aligned SWNTs, in which the Al_2O_3 buffer layer can inhibit the coarsening of Fe catalyst particles, the presence of the buffer layer on the top or bottom of catalyst layer raises other problems when SWNTs are used in electrical devices, such as adhesion, electrical conductivity and impurities. Accordingly, the purpose of this work was to develop a process to

fabricate the well-aligned SWNTs at low temperatures without buffer layer application. The idea is to use the catalyst precursor (CoCrPtO$_x$) to promote the miniaturization of nanoparticles and to prevent the agglomeration effect during pretreatment and the initial stage of CNTs growth.

Chapter Ⅱ
Literature review

2.1 Structures and properties of CNTs

Since discovery of CNTs in 1991 [Iijima-1991-56], many superior properties of CNTs have attracted much attention of the scientists. The excellent properties of CNTs must be closely related to its unique structure. It was proposed that a graphene sheet of (0001) plane can be rolled to become various forms of CNTs structures: armchair, zigzag and chiral CNTs. The CNTs can be pictured as the fullerene-related structures with the end caps containing pentagon and hexagon rings. As shown in Fig.2.1 [Dresselhaus-1996-p756], if a C_{60} structure is bisected normal to a five-fold axis, the "armchair" tubule can be formed. 'Zigzag' tubule is formed in the way of bisecting C_{60} structure normal to a three-fold axis. The other ways of bisecting C_{60} structure can form the chiral CNTs. The caps of C_{60}, C_{70} and C_{80} [Fig. 2.1(a)] are corresponding to the CNTs structures in armchair, zigzag and chiral, respectively [Figs. 2.1(c) and 2.1(d)]. In mathematics, scientists proposed a vector to define CNTs [Saito-92-2204]:

$$C_h = na_1 + ma_2 \equiv (n,m)$$
(2-1)

The C_h called chiral vector, and the angle between C_h and a_1 is chiral angle θ,

while a_1 and a_2 denoted the unit vectors of graphene sheet. As shown in Fig. 2.2, the structures of CNTs in zigzag, armchair or chiral form are classified by the θ angle or range, i.e. 0°, 30° or $0^o < \theta < 30^o$, respectively. The chiral vector is expressed as a pair of integers (n, m) for mapping planar graphene sheet. The zigzag, armchair and chiral CNTs are corresponding to the chiral vectors of (n, 0), (n, n) and (n, m), respectively.

In 1992, Hamada and Saito [Hamada-1992-1579] [Saito-1992-2204] proposed theoretically that the CNTs can be a conductor or a semiconductor depending on its chirality. Their theories were proved experimentally by Wildoer and Odom [Wildoer-1998-59] [Odom-1998-62] in 1998, using STM. They indicated that the two parameters, helicity and diameter, can be adopted to distinguish the metallic from semi-conducting properties of CNTs, i.e. the differences in the band gap and the Fermi energy shift. Among them, the armchair CNTs have two integers n and m equal to each other, thus have bands that cross the Fermi level and therefore are truly metallic. The chiral and zigzag nanotubes had two possibilities: (a) If n-m = 3k, where k is a integer except zero, then it was metallic with an energy gap of about 1.7 - 2.0 eV; (b) If n-m $\neq$ 3k, then it was semiconducting with an energy gap of about 0.5 - 0.6 eV [Fig. 2.3]. These show the nanotubes electrical properties are very sensitive to the wrapping angle and the tube diameter. Ballistic transport in the CNT channel was assumed.
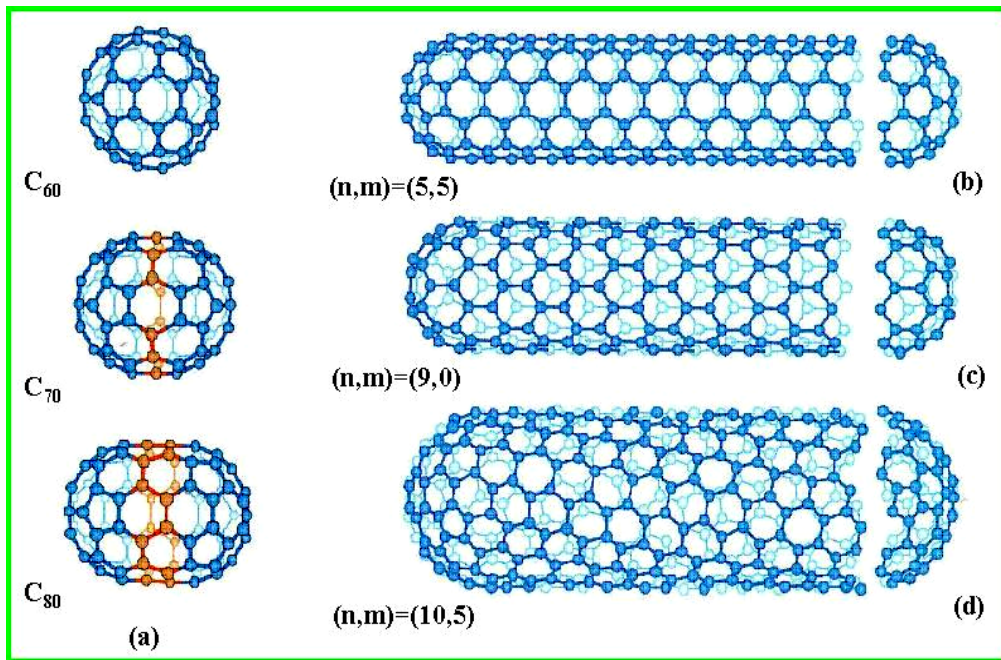
Fig. 2.1 CNT structures of armchair, chiral and zigzag tubules.[Dresselhaus-1996-p756]
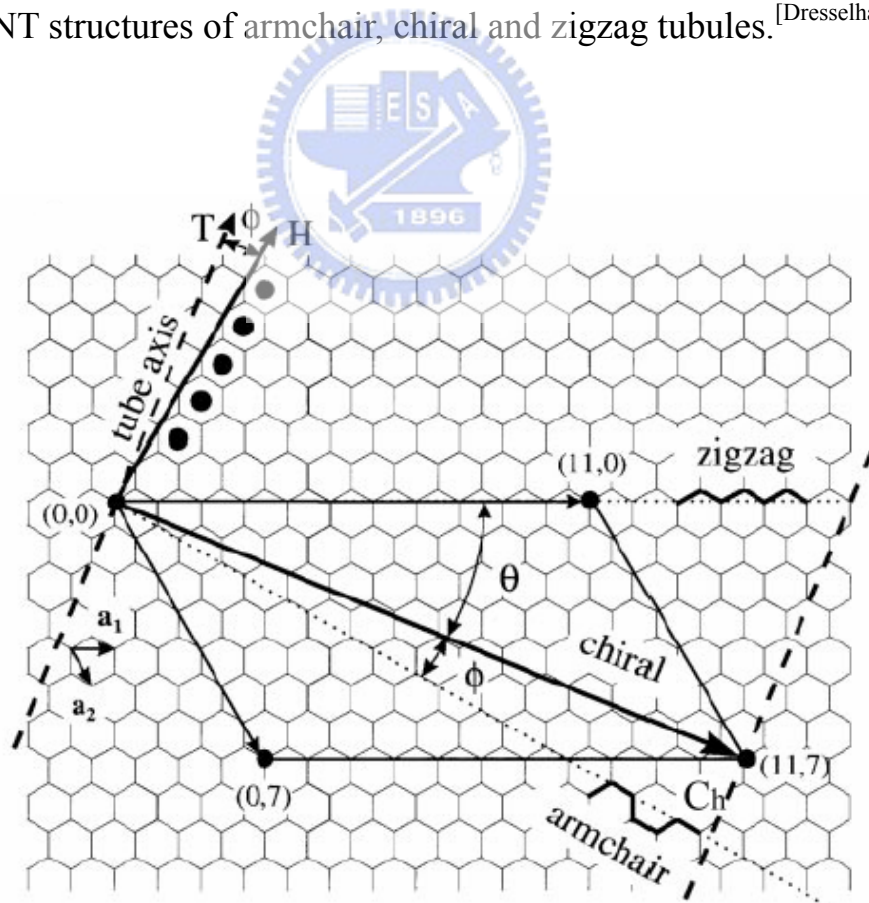
Fig. 2.2 The construction of CNT from a single graphite sheet[Saito-1992-2204]
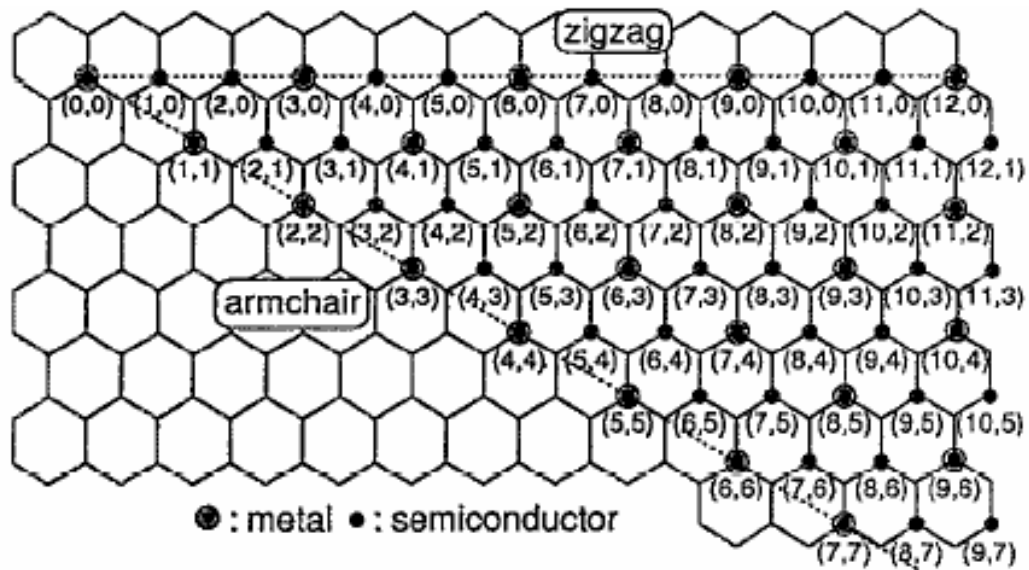
Fig. 2.3 The relation between properties and structure of CNTs[Saito-1992-2204]

In addition to the special features on electrical properties of CNTs, another key point of what scientists concerned is their field emission properties. The field emission is an electron emission phenomenon through tunneling effect when an electric field is applied on the surface of a material with negative potential. Due to suitable geometric contours, high thermal stability, good mechanical strength and high chemical stability, CNTs becomes a good field emission material. The field emission is much more fascinating than thermal emission since it just needs to apply a low electrical field (~V/μm) at room temperature. Usually, the field emission properties can be expressed by Fowler-Nordheim equation [Spindt-1976-5248] :
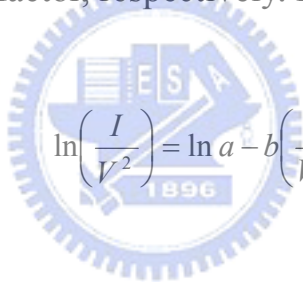
$$I = aV^2 \exp\left(\frac{-b}{V}\right) \tag{2-2}$$

$$a = \frac{\alpha A \beta^2}{1.1\phi} \exp\left[\frac{B\left(1.44 \times 10^{-7}\right)}{\phi^{1/2}}\right] \tag{2-3}$$

$$b = \frac{0.95 B \phi^{3/2}}{\beta} \tag{2-4}$$

$$\text{with} \quad A = 1.54 \times 10^{-6}, \quad B = 6.87 \times 10^{7} \tag{2-5}$$

where I, V, ϕ, α and β are the field emission current (A), an applied

voltage (V), a work function of material (eV), the effective emission area (m^2),

and the field enhancement factor, respectively. Base on Eq. 2-2, one can obtain：

$$\ln\left(\frac{I}{V^2}\right) = \ln a - b\left(\frac{1}{V}\right) \tag{2-6}$$

The $\ln(\frac{1}{V^2})$ versus $\frac{1}{V}$ curve is called F-N plot. A material with good field

emission properties often shows a negative slope on the F-N plot. Base on Eq.

(2-2), the ways to improve the field emission properties of a material can be

achieved by increasing the effective emission area, α, and the field emission

factor, β, which is related to the aspect ratio or geometric factor of emitter.

Furthermore, the too-close distance between emitters can deteriorate their

emission properties, which is often called the screen-effect. [Gröning-2000-665] This

signifies that the manipulation of the tube number density is also an important

issue in field emission studies.

In addition to special marvelous electrical properties, the mechanical properties, e.g. the reported Young's modules may reach over 1 TPa [Eric-1997-1971] which makes CNTs the stiffest material in the world. CNTs also behave elongation to failure of 20-30% [Pan-1999-3152] with a high tensile strength about 60 GPa[Yu-2000-637]. These experiment values enable the CNTs to become the highest strength/weight ratio material on earth, and to be used for potential applications in reinforcement of the composites.

Furthermore, thermal manage is now a very hot research in the world and the thermal conduction of CNTs are also excellent. Che et al. [Che-2000-65] evaluated thermal conductivity of 10-nm-long CNTs are great than 2800 W/mK, almost equal to diamond. Berber et al. [Berber-2000-4613] predicted the thermal conductivity of (10,10) SWNT is about 6600 W/mK at room temperature. This is a very important support for their electronic and thermal applications.

2.2 Synthetic methods of SWNTs

There are many methods being developed to synthesize SWNTs, where arc-discharge, laser ablation and chemical vapor deposition (CVD) are the most popular methods [Lee-2001-245]. In those methods, carbon sources can be in gas or solid phases. The morphology and properties of SWNTs are often controlled by manipulating the following process parameters: substrate temperature, precursor

gases and gas ratio, catalyst, pretreatment conditions, applied bias, etc. However, the proposed methods still suffer the following problems: low yielding, low uniformities in structure and property, etc.

(a) Arc-discharge method[Saito-1995-33]

Arc-discharge method is believed to be the earliest way to synthesize CNTs. When CNTs were first identified by Iijima[Iijima-1991-56], it was produced by this method. Figure 2.4 shows the schematic diagram of the arc-discharge system [Saito-1995-33]. There are two graphitic rods as anode and cathode. Between these two electrodes, arcing occurs when DC voltage is applied. In the situation of anode containing small amount of catalyst such as Fe, Co, Ni and Y, the SWNTs can be synthesized[Bethune-1993-605], and MWNTs can be fabricated by using pure graphite as two electrodes. Generally, the discharge is operated at a voltage range between 20 and 40 V with current from 40 to 100 A under He or Ar atmosphere of 10-500 Torr. Carbon clusters collided out from the anodic graphite rod by electron bombardment are deposited on the cathode surface. The production on cathode may include amorphous carbon, fullerenes, carbon cluster, carbon nanotubes and varieties of other carbon structures. Therefore, purification of the nanostructures is generally an important issue for applications. Another drawback of this process is its low yielding in producing CNTs.
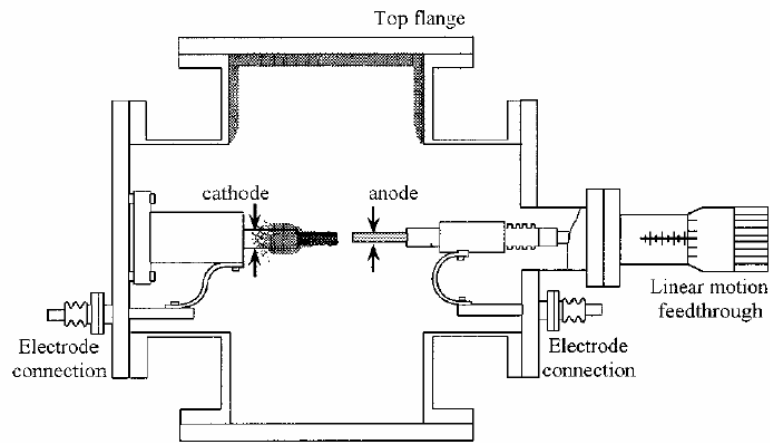
Fig. 2.4 Schematic diagram of arc-discharge system [Saito-1995-33]

(b) Laser ablation[Guo-1995-49]

Laser ablation method was first reported by Guo's group in 1995[Guo-1995-49], as shown schematically in Fig. 2.5. There is an incident laser beam for vaporizing graphite target under helium or argon gas atmosphere at pressure of 500 Torr. The productions are swept out by the flowing gas and to be deposited on the water cooled collector. Therefore, it is also called laser vaporization method. The graphite target containing Co, Ni, Fe, or Y is a more favor condition to form SWNTs.
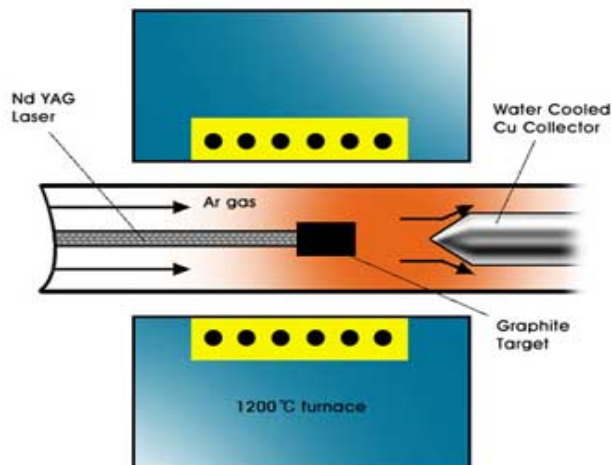
Fig. 2.5 Schematic diagram of laser ablation system [Guo-1995-49]

(C) Chemical vapor deposition (CVD)

The CVD method is a mature technique in thin film processes. Most of films can be fabricated by CVD method, including metals, semiconductors and insulators. It is essential for CVD process to introduce some forms of the energy to decompose precursor gases and deposit the reaction product on the substrate surface. The introduced energy may include thermal, microwave, RF, or others. Thus, it gives rise to different process names, depending on the source of the applied energy.

(1) Thermal chemical vapor deposition: [Lee-2001-245]

Figure 2.6 shows a schematic diagram of thermal CVD apparatus in the synthesis of carbon nanotubes. The method was used pyrolysis of hydrocarbon source to synthesize the SWNTs. This method is also catalyst assisted SWNTs growth method and the quality of SWNTs is sensitive to the pyrolysis temperature. The specimen is placed in a quartz boat with coated transition metals or theirs alloy on a substrate, and then the boat is positioned in a CVD reaction furnace, and nano-size fine catalytic metal particles are formed after an additional etching of the catalytic metal film with NH_3 gas at a temperature in 750 to 1050°C. Reaction gas is supplied in one end of the apparatus, and gas outlet in the other. The merit of this method is easily to deposit large area, uniform and good quality of SWNTs. However the drawback is not compatible

with IC (integrated circuit) process due to working temperature over 600°C.
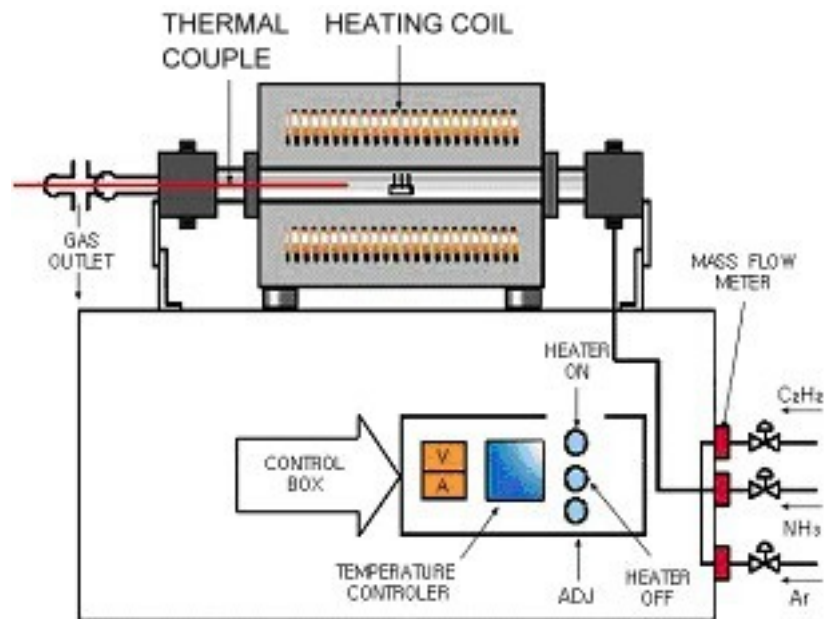
Fig. 2.6 Schematic drawings of thermal CVD system [Lee-2001-245]

(2) Plasma enhanced CVD (PECVD): [Qin-1998-3437]

PECVD system was employed to deposit the SWNTs with many merits

comparing with other methods, e.g. compatible process with IC process, cheaper,

less contamination, high yielding and controlled alignment of SWNTs, thus

current attention has focused on developing new techniques for the preparation

of vertically aligned SWNTs by using CVD methods.

According to the methods of plasma excitation can be classified the

different plasma system such as microwave plasma CVD (MPCVD), RF or DC

bias excited plasma CVD (PECVD), microwave plasma assisted hot filament

CVD (MP-HFCVD) and electron cyclotron resonance CVD (ECR-CVD) and so

fourth. Generally, the power supplies for discharge of plasma CVD are DC bias; radio frequency (RF) (13.56 MHz) and microwave (2.47 GHz) are typical of high frequency power supply. Using the plasma CVD process to produce SWNTs can be prepared by applying decomposition of hydrocarbon (such as CH_4, C_2H_2, C_2H_4 and C_6H_6) or monoxide and even decomposed of metal complex on various substrates that coated transition-metal film.

The common used of microwave plasma CVD, such as MP-CVD, PE-HF-CVD, and ECR-CVD, to synthesize SWNTs can be ranked in terms of their working pressure, where MP-CVD or PE-HF-CVD and ECR-CVD were operated with the pressure range of $P < 10^{-3}$ Torr and $10^{-1} < P < 100$ Torr, respectively. The MP-CVD system [Qin-1998-3437] as shown in Fig. 2.7, with the high density of plasma ball permits a contamination-free and a modification of plasma shape through tuning of the cavity. The PE-HF-CVD system applied the current on the tungsten filament to efficiently increase temperature in the chamber [Kurt-2001-1723] as shown in Fig. 2.8 The ECR-CVD as shown in Fig. 2.9 is known for its own advantages of high dissociation percentage of the precursor gas, high uniformity of plasma energy distribution and large area of CNTs deposition [Tsai-2001-NCTU].
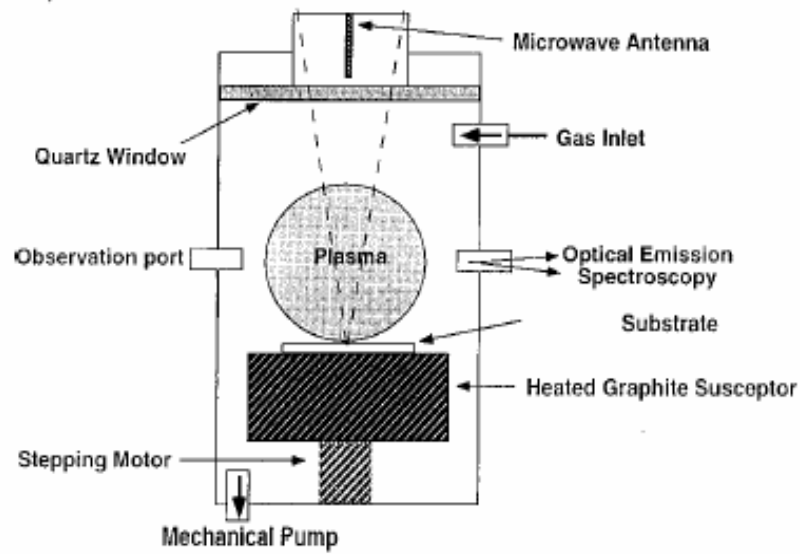
Fig. 2.7 Schematic drawing of MPCVD apparatus [Qin-1998-3437]
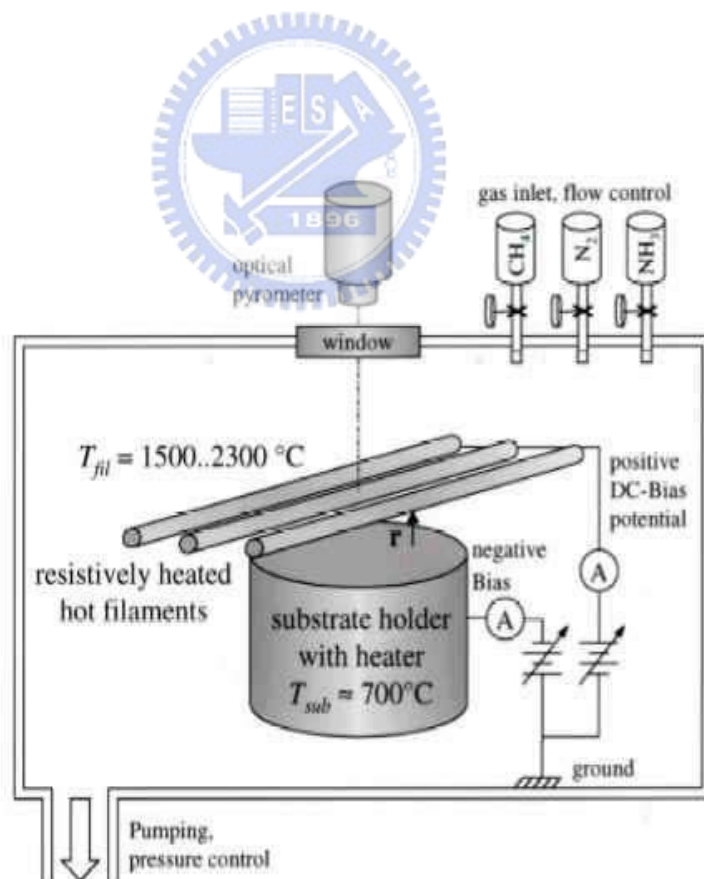
Fig. 2.8 Schematic drawing of PE-HF-CVD apparatus [Kurt-2001-1723]
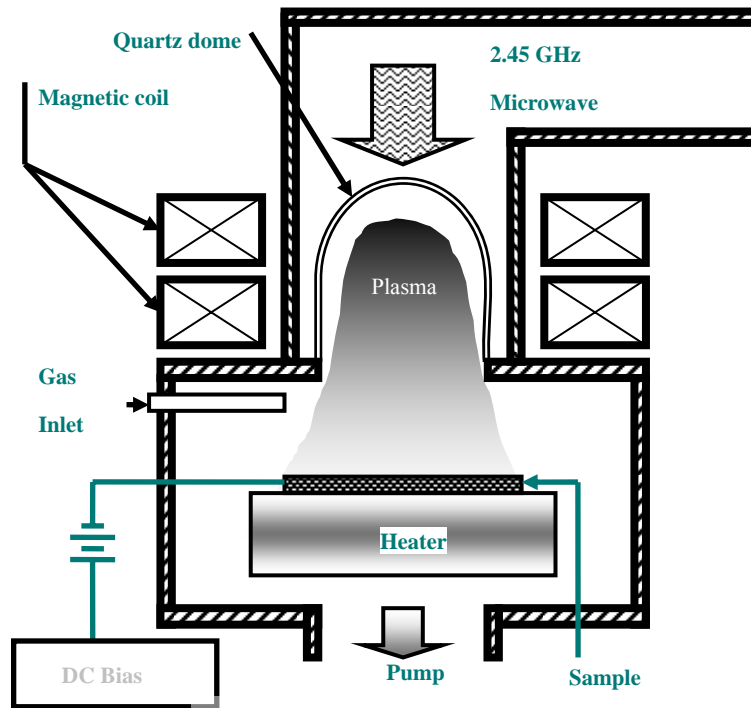
Fig. 2.9 Schematic drawing of MPCVD apparatus [Tsai-2001-NCTU]

(d) Buffer layer-assisted growth of SWNTs

Buffer materials are most effectively to promote SWNTs formation. Wang et al. [Wang-2006-in press] demonstrate that AlON buffer layer is the best material for SWNTs fabrication. Moreover, the results also indicate that the favorable conditions for synthesizing SWNTs networks are a high substrate temperature, low CH_4/H_2 ratio and thin catalyst thickness with AlON as the buffer layer material. The roughness of AlON film is presenting a rough (~1 nm) surface [Fig. 2.10], whereas Si wafer surface is quite neat. These results suggest the protrusion on rough buffer layer (e.g., AlON) can cause instabilities on Co

17

catalyst surface and form nuclei sites for tubes growth afterwards. They also

have measured the roughness of other buffer materials, such as AlN, TiN, and

TiO$_2$. The results show their surface are quite smooth and roughness (R$_{rms}$) are

on the order of angstroms at most, show hardly effect to enhance SWNTs.

Figure 2.11 shows the growth processes of buffer layer assisted growth of

network SWNTs.
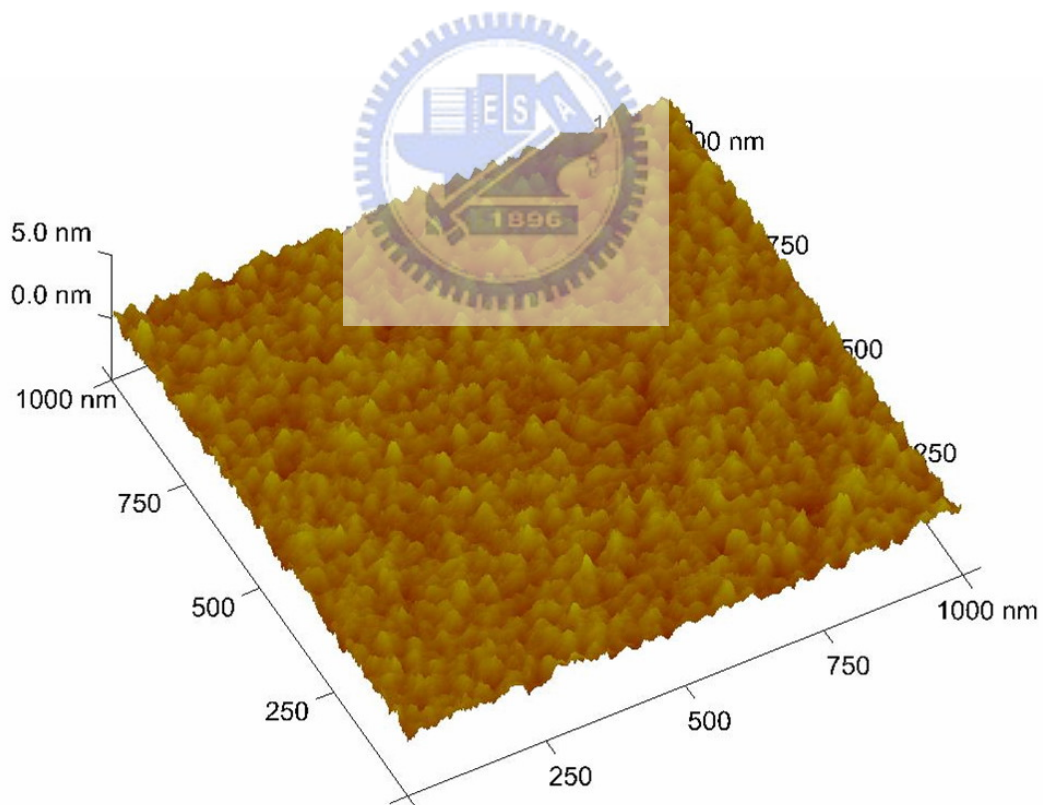
Fig. 2.10 AFM image of AlON buffer layer of 10 nm where shows rough surface. The rms value of surface roughness is about 1.0 nm. [Wang-2006-in press]
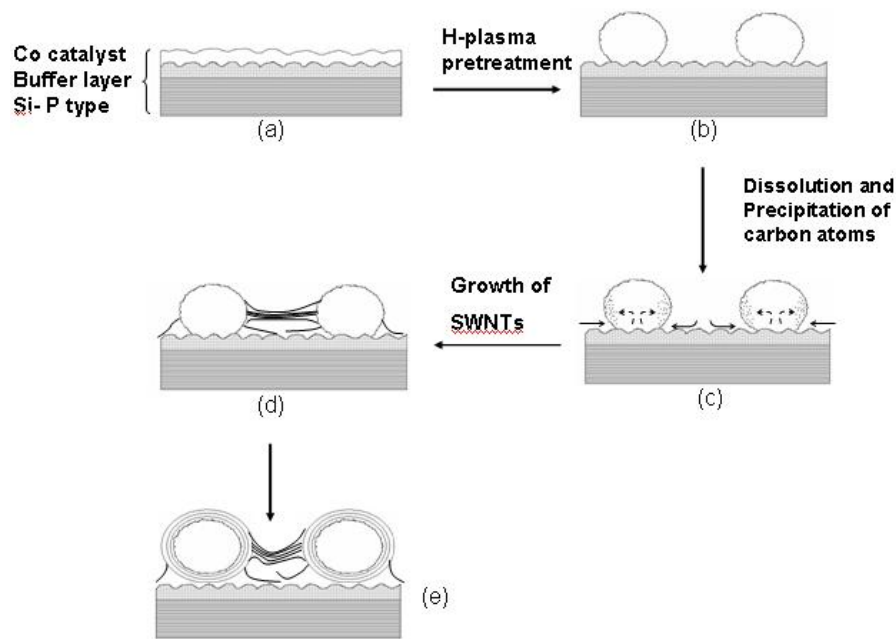
Fig. 2.11 Schematic diagram of the growth processes of SWNTs networks assisted by buffer layer. [Wang-2006-in press]

(e) Alloy catalyst-assisted growth of SWNTs

Alloy catalysts were recently employed to growth CNTs like CoMo, FeNi, CoPt, FePt [Kuo-2003-799] and so on. But no extremely dense vertically aligned SWNTs were grown by alloy catalysts in the past. PtO_x has been recently used in optical storage media and nonvolatile memory technology because of its explosive effect of the decomposition of PtO_x at an appropriate process temperature. Kim et al. [Kim-2003-1701] proposed that PtO_x film will decompose to Pt nano-particles and O_2 by laser thermal pretreatment. The decomposition temperature is approximately $500°C$ (1 atmosphere in air). Figures 2-12(a) and 2-12(b) show that PtO_x film was self-assembled to nano-particles by laser pretreatment and then transmittance is decreased (reflectance is increased) by

19

the decomposition of PtO_x film to Pt nano-particles and O_2 [Fig. 2.13]. Thus, it is so interesting to adopt PtO_x with other metals, like Co and Cr, to be alloy-catalyst for synthesis of SWNTs.
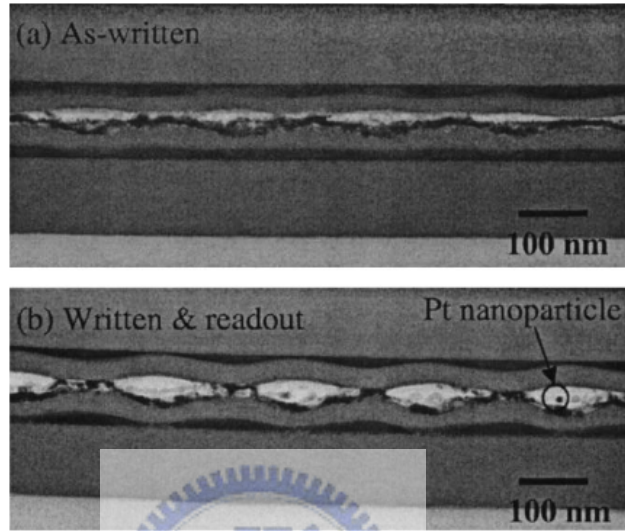
Fig. 2.12 TEM images of (a) PtO_x thin film and (b) self-assembled Pt nanoparticles after laser pretreatment. [Kim-2003-1701]
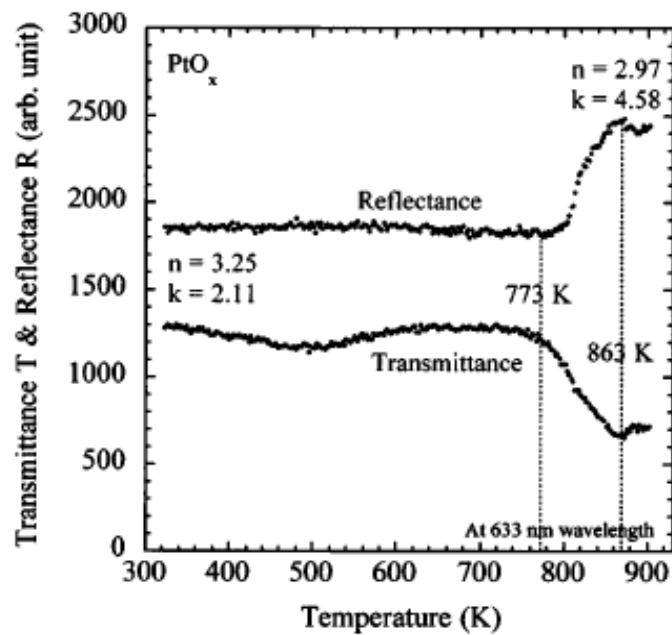
Fig. 2.13 Thermo-optical properties of PtO_x single layer. [Kim-2003-1701] (n: refractive index, k: extinction coefficient).

2.3 Growth mechanisms of SWNTs

Regarding the use of CVD methods for SWNTs growth, many growth mechanisms have been proposed[]. However, most of the mechanisms are based on the original model of carbon nanofibres proposed in 1970s by Backer. [Backer-1978-14] It is believed that nanotubes grow as carbon precipitates from a supersaturated metal catalyst that resides at either the base or the tip of a growing nanotube. Catalyst/substrate interactions and temperature gradients across the catalyst particle are considered to be important factors that determine the growth mechanism. Catalyst size was believed to determine the CNT diameter, and SWNT was synthesized when catalyst size is about 1~2 nm. However, most of these models were proposed without sufficient and systematic supporting experimental evidence, and they often lacked details about the physical mechanisms and the effects of various process parameters. Thus, the kinetics of nanotube nucleation and growth are not well known yet. Other growth mechanisms are described as follows:

(a) Ball-and-stick catalyst scooting model [kuo-2004-p.9-10]

Birkett et al. [Birkett-1997-111] proposed that transition metals show a high propensity for decoration fullerene surfaces. A carbon fragments bind to the metal clad fullerene and they may self-assemble as a surrounding circular hexagonal chicken-wire-like fence. Once formed as a belt, the network could

propagate as a cylinder, so called open edge growth. This model predicts the SWNT diameter will be $d(C_{60}) + 2*d$(Interplanar distance), i.e. 0.7 nm + 2(0.34) nm = 1.38 nm ,which is in excellent agreement with observation. Another possible model was scooter mechanism[Thess-1996-483] which considered that a few metal atoms chemisorbed and scooted around the open edge of the sheet and kept tube open and grow. When metal atoms aggregated and lost its kinetic energy for scooting, SWNT growth will stop. Figure 2.14 shows the schematic diagram of ball-and-stick scooting model.
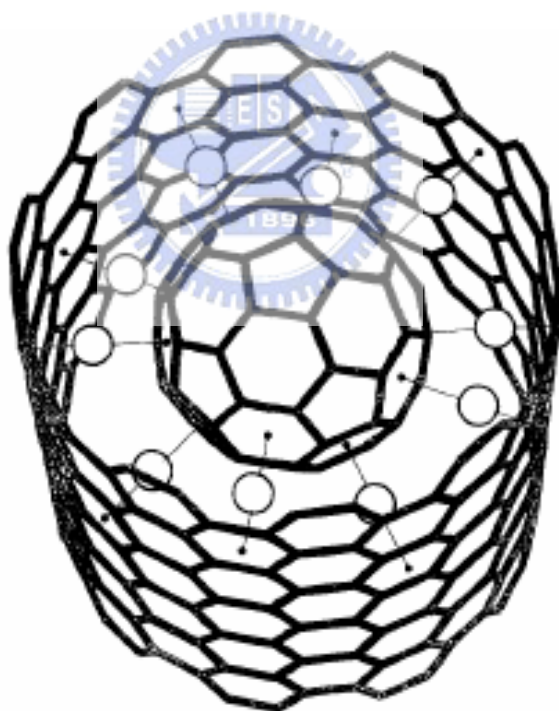
Fig. 2.14 Schematic diagram of ball-and-stick scooting model [Birkett-1997-111]

(b) Root growth mechanism

When numerous SWNTs grow by a single catalyst particle and their

diameter are much smaller than catalyst, this is called root growth mechanism. Saito et al.[saito-1994-L526] proposed that when catalyst metal is evaporated together with carbon by arc discharge, carbon-metal alloy particles are formed on the cathode surface. Since the carbon-metal compound soot was produced in a carbon-rich at atmosphere, the initial alloy particles in a liquid phase contained more carbon than solubility limit in a solid state. Therefore, with the decrease of temperature of the cathode, the liquid alloy particles begin to segregate excess carbon on their surfaces. When the cooling of particles proceeded at a moderate rate and the supersaturation of carbon in metal particles was not so high, the carbon gradually segregated on the surface and formed graphitic layers one by one. When cooling was rapid and the initial content of carbon in a particle was high compared with that in the process mentioned above, the supersaturation of carbon became rather high. According to the classical nucleation theory, high supersaturation would bring about nucleation of graphite at numerous sites on the surface of a particle. Since the formation of flakes of graphitic occurs suddenly, a large number of tiny graphitic flakes are formed. These flakes curl and then close their open ends in order to saturate dangling bonds at their periphery. Among this random assembly of graphitic flakes, seeds of SWNTs may be formed [Figs. 2.15 and 2.16].
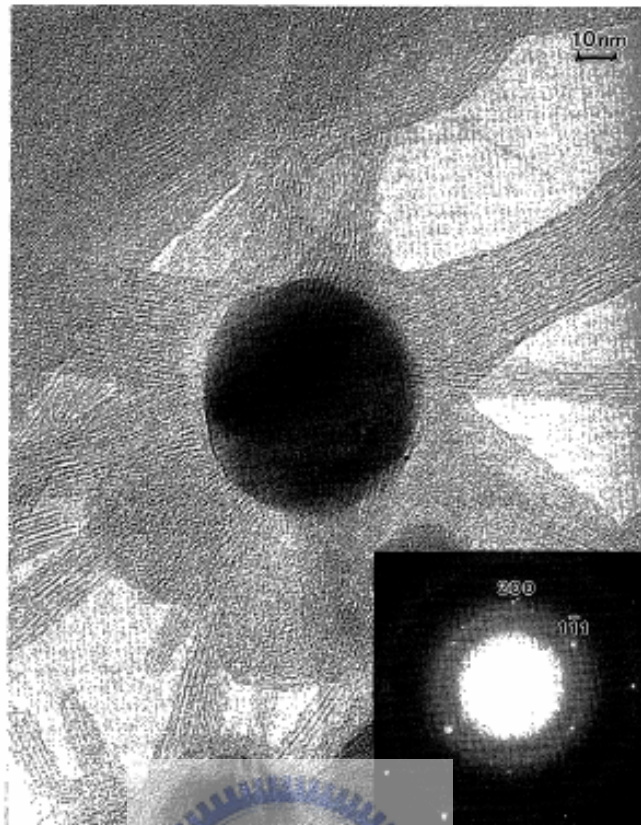
Fig. 2.15 TEM image of radiate sea-urchin-like SWNTs [saito-1994-L526]
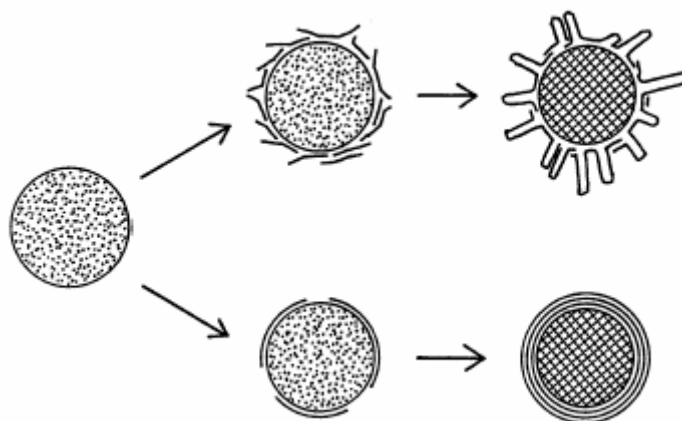
Fig. 2.16 Schematic diagram of root growth mechanism -1 [saito-1994-L526]

Zhou et al.[zhou-1994-1593] proposed another model that SWNTs was separated

from catalyst surface by graphite layers, as shown in Fig. 2.17. Furthermore,

Gavillet et al[Gavillet-2001-275504] suggest a common growth mechanism based on a vapor-liquid-solid model. The first step of the process is the formation of a liquid nanoparticle of metal supersaturated with carbon [Fig. 2.18(a)]. And then there is a competition between the formation of a graphitic sheet [Fig. 2.18(b)] and the nucleation of single-wall nanotubes [Fig. 2.18(c)]. In order to obtain long nanotubes [Fig. 2.18(d)], the root-growth process should continue for a sufficiently long time, until local temperatures are too low, leading to the solidification of the nanoparticles. Figures 2.18(e) and 2.18(f) show that nucleation did occur but growth did not take place so that carbon has partly condensed into amorphous carbon flakes or into a few graphitic layers.

Fig. 2.17 TEM image of the interface between the multilayered cage and the single-walled tubes [zhou-1994-1593]
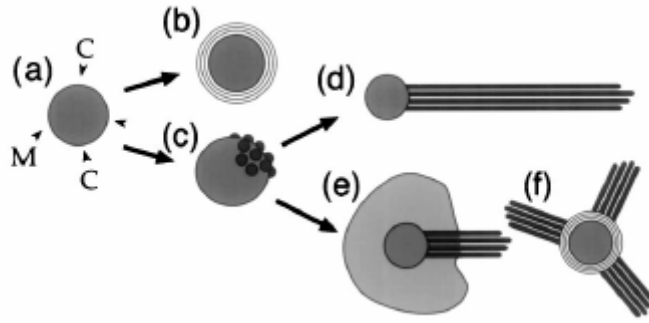
Fig. 2.18 Schematic diagram of root growth mechanism -2 [Gavillet-2001-275504]

(c) Yarmulke mechanism

This model was proposed by Dai et al.[Dai-1996-471] that SWNTs are formed

on molybdenum nanoparticles in the size range of 1~4 nm by the

disproportionation of CO at 1200°C, indicates that there can be a slight variation

in the size. And they observed that SWNTs were close end and the catalysts

were on the top of tubes. So yarmulke mechanism was supposed that carbon

atoms were chemisorbed on the catalyst to form yarmulke firstly. And then

carbon source decomposed and diffused into catalyst, so that SWNTs grew

longer. In the case of organometallic precursors, it seems that SWNTs of ~1 nm

diameter are produced under controlled conditions. When the organometallic

concentration is high, MWNTs are formed around the catalyst particles with

sizes in the range of 5~20 nm. In the larger size range, >50 nm, graphite-covered

metal particles are predominantly formed [Fig. 2.19].
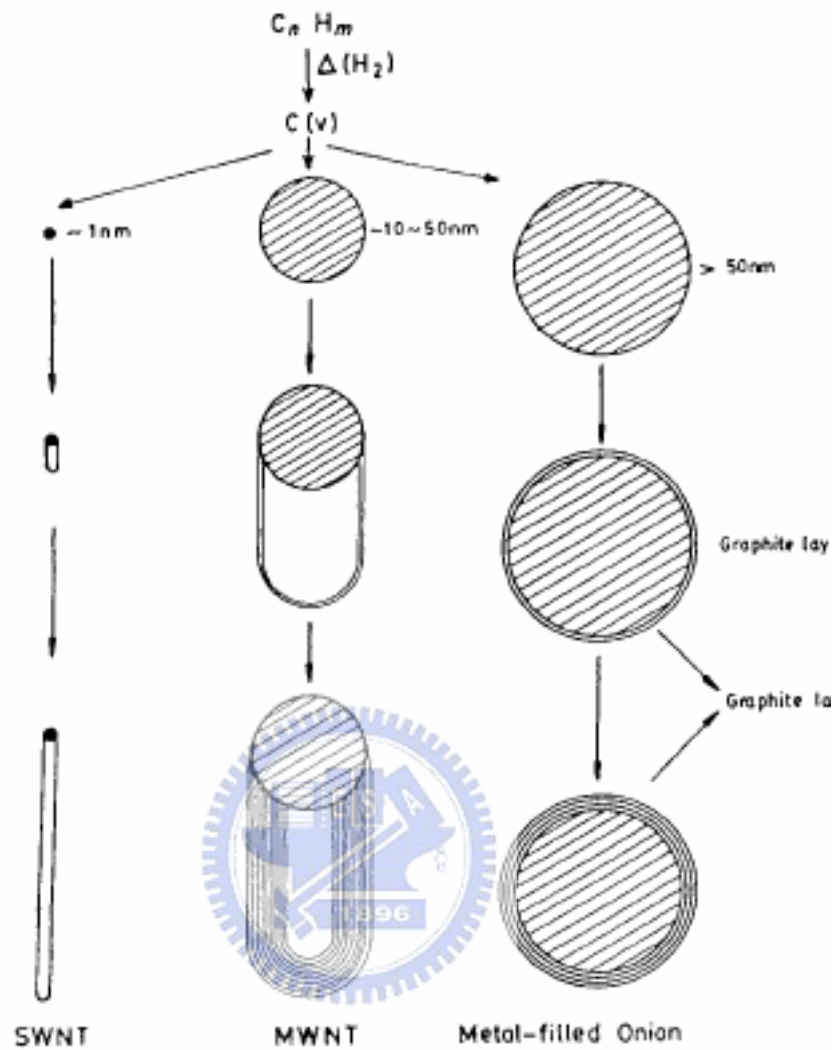
Fig. 2.19 Schematic diagram of Yarmulke mechanism [Dai-1996-471]

(d) Solid–liquid–solid growth mechanism

Gorbunov et al.[Gorbunov-2002-113] proposed that a molten catalyst nanoparticle penetrates an amorphous carbon aggregate dissolving it and precipitating carbon atom [Fig. 2.20(a)]. These atoms arrange in a graphene sheet [Fig. 2.20(b)], whose orientation parallel to the supersaturated metal-carbon melt is not

27

energetically favorable. Any local defect of this graphene sheet will result in its

buckling [Fig. 2.20(c)] and formation of a SWNT nucleus [Fig. 2.20(d)]. Further

precipitating carbons incorporate in edges of growing nanotube [Fig. 2.20(e)]

which are anchored to the catalyst nanoparticle by overlapping its unsaturated

sp^2 orbitals with the metal orbitals of the catalyst nanoparticles.
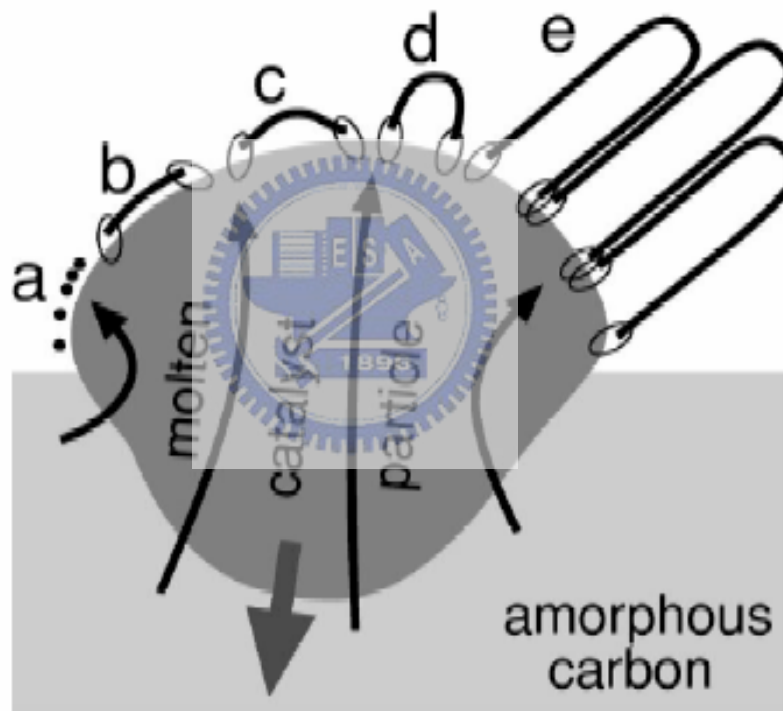
Fig. 2.20 Schematic diagram of Solid–liquid–solid growth mechanism
[Gorbunov-2002-113]

2.4 Process parameters of SWNTs growth in MP-CVD

Different parameter can result in distinct properties of SWNTs e.g.

morphology, growth mechanism, tube number density, structure, etc.

(a)Catalyst：

Different catalysts own distinct properties and the growth of SWNTs can be affected. If a catalyst particle is tightly sintered, it becomes harder to melt during reduction or pretreatment process. In other words, to form nano-scaled liquid droplets which provides the embryo of SWNTs is more difficult, so the same catalyst leads to the growth of nano-sheet instead of nanotube with lower growth temperature.[Lin-2002-922] The ways of depositing catalyst also cause influences as well.

(b)Growth temperature：

Besides the above-mentioned influence of catalyst reduction, temperature can also affect the diffusion rate of carbon atoms inside the catalyst. With higher growth temperature, the diffusion rate within catalyst becomes quickly and direct affects the growth rate, length and tube number density of CNTs. Also, the precursor gases decompose amount can be different with different temperature. It changes the mixing concentrations of precursors. In addition, the crystalline of graphene layer becomes better with higher growth temperature.

(c)Gas

This condition includes precursor type, flow rate and gas ratio. In literature, many carbon source and reducing gas has been used. [Yun-2003-6789] [Lin-2002-922] Different gas types have distinct pyrolysis temperature and different

bombardment effect in plasma environment.

(d)Working pressure：

When the inlet and pumped out gas flow reach a steady state, the pressure in chamber is called working pressure. The main effects of this parameter are the plasma behavior. With higher pressure, the mean free path of radical decrease but collision probability increase. The plasma induced self-bias will change with different pressure.

(e)Growth time：

Growth time usually changes the length of SWNTs. But after catalyst is poisoned, the growth time won't affect it any more.

2.5 Analyses of SWNTs

(a) Raman spectroscopy analysis

(1)Measurement principle[Rao-1997-187]

Raman spectroscopy provides information about molecular vibrations that can be used for sample identification and quantitation. The Raman effect arises when a monochromatic light (laser) shines on a sample and excites molecules in the sample, which subsequently scatter the light. While most of this scattered light is at the same wavelength as the monochromatic light, some （±0.0001%) is scattered at a different wavelength. This in elastically scattered light is called

Raman scatter. It results from the molecule changing its molecular motions. The

energy difference between the monochromatic light and the Raman scattered

light is equal to the energy involved in changing the molecule's vibrational state.

This energy involved in changing the molecule's vibrational state. This energy

difference is called the Raman shift. Several different Raman shifted signals will

often be observed; each being associated with different vibrational or rotational

motions of molecules in the sample. Figure 2.21 shows the schematic diagram of

state change of Raman scattering.
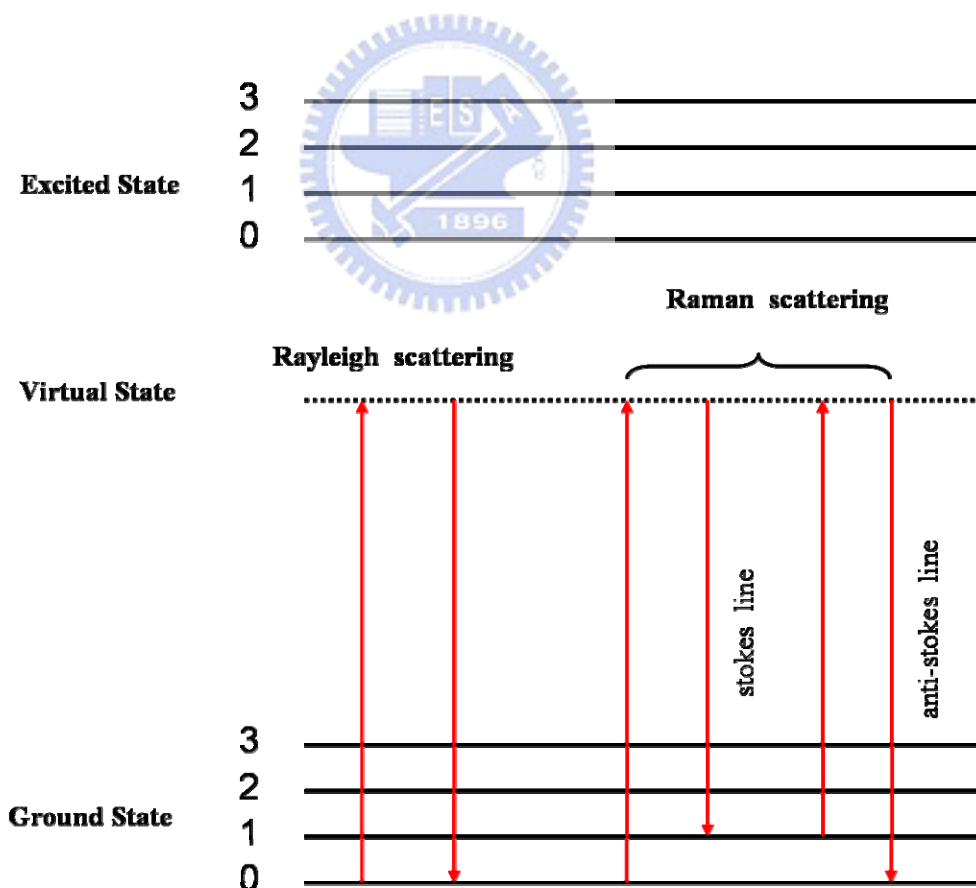
Fig. 2.21 Schematic diagram of state change of Raman scattering[Rao-1997-187]

(2)Raman shifts of SWNT[Raravikar-2002-235424]

SWNT has 15 or 16 Raman-active modes, but some of their Raman scattering are difficult to detect, so only 7 Raman-active modes can be observed in measurement, as shown in Fig. 2.22.

Figures 2.23(a) and 2.23(b) show a typical Raman spectrum of SWNT sample taken at room temperature. The two prominent peaks with a peak position of 182 and 264 cm^{-1} in Fig. 2.23(a) are the two RBM (radial breath mode，A_{1g}) peaks. The two peaks from Fig. 2.23(b) at peak positions ~1590 and ~1350 cm^{-1} belong to the G-band (tangential stretching mode，E_{2g}) and D-band (from amorphous carbon，A_{1g}), respectively.

Figures 2.24(a), 2.24(b) and 2.24(c) show the G-band, D-band vibrational modes and the RBM's in SWNTs respectively. In graphite and CNTs, the G-band Raman vibrational modes are present due to the in-plane vibrational movement of carbon atoms, which involves a combination of stretching and bending of the carbon-carbon (C-C) bonds. The disorder-induced D-band Raman vibrational mode, which is a highly dispersive spectral feature, is also present in these materials due to the collective in-plane vibrational movement of atoms towards and away from the center of the hexagons formed by the covalently (sp^2) bonded carbon atoms. Therefore, the D-band mode involves stretching and bending of C-C bonds.

The RBM is a unique feature in the Raman spectrum of SWNTs and involves a collective vibrational movement of the carbon atoms towards and away from the central axis of a SWNT. The RBM oscillations are associated with a periodicity imposed on a graphene sheet by wrapping it into a finite-size (small diameter) tube. Consequently, the associated RBM Wavelength and frequency are directly related to the perimeter of the nanotube. Base on this relationship, as the diameter of the nanotube increases, the RBM frequency shifts to lower wave numbers. For larger and, particularly, MWNTs, the RBM frequency becomes very small and, at the same time, the intensity of the radial breathing mode decreases and ultimately becomes undetectable by Raman spectroscopy measurements. Hence Dresselhaus et al. [Dresselhaus-2002-2043] proposed that the frequency of the RBM are：

$$\omega = ä(cm^{-1}\ nm)/d(nm) \qquad\qquad (2\text{-}7)$$

where ä for the Si /SiO substrate is experimentally found to be 248 cm^{-1}nm for isolated SWNTs, ω is the peak position, d is the SWNT diameter and RBM is independent of chiral angle. Furthermore, Tuinstra et al. [Tuinstra-1970-1126] proposed that the Raman spectra of single crystals of graphite shows only one mode at 1575cm^{-1} and as the increase of defects and disorder, D-band will show, so the I_G/I_D ratio can be used to determine the graphitized degree of SWNTs.
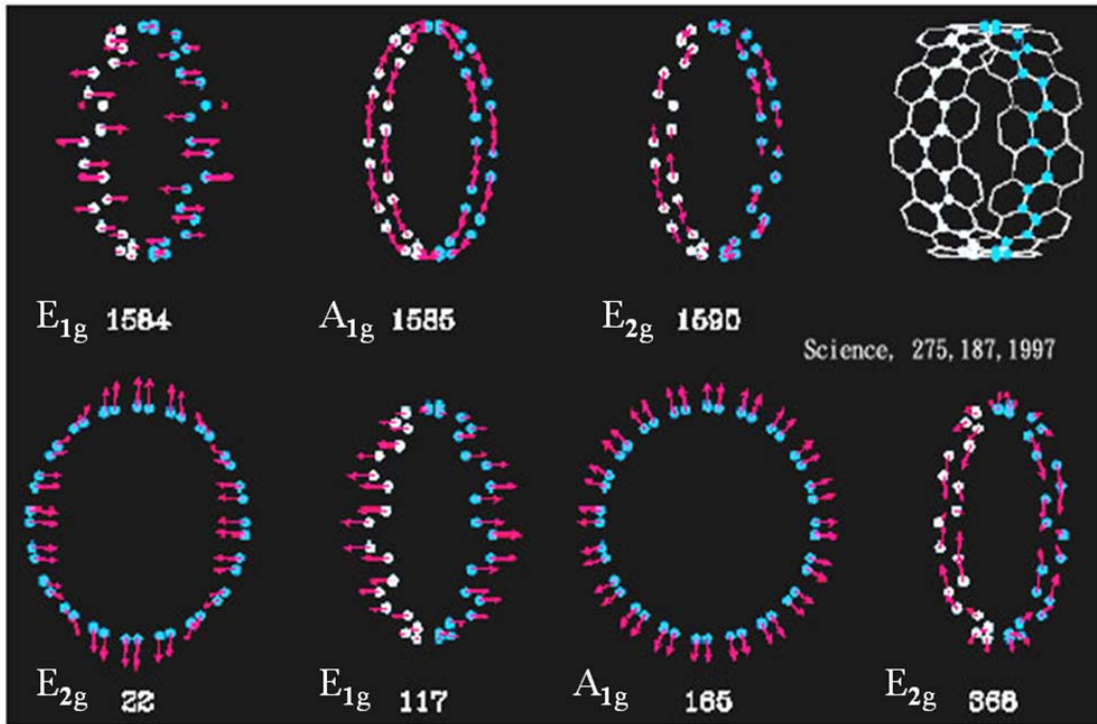
Fig. 2.22 Raman-active normal mode eigenvectors and frequencies for a (10,10) nanotube [Rao-1997-187]
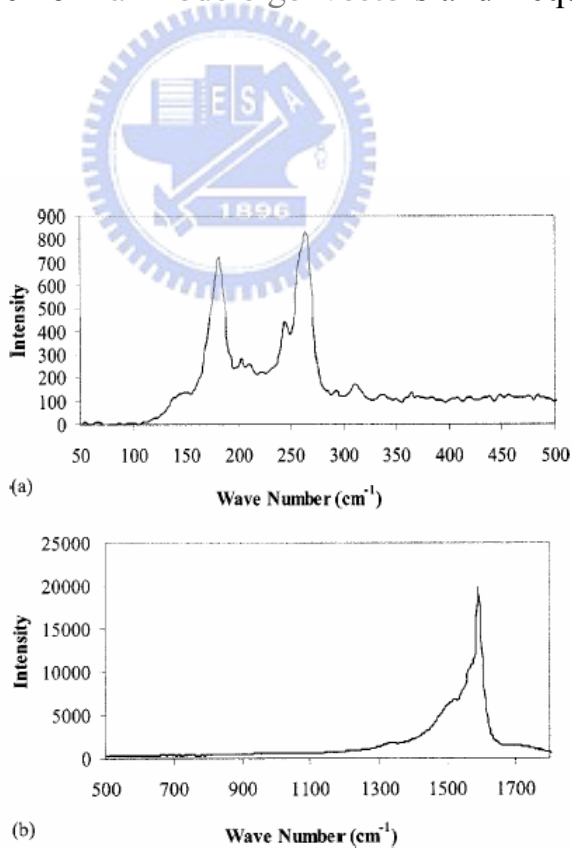
FIG. 2. Standard room-temperature Raman spectrum of as-received HiPco SWNTs taken at $E_{laser}=2.41$ eV. (a) Raman spectrum showing RBM peaks. (b) Raman spectrum showing G-band and D-band peaks.

Fig. 2.23 Raman spectra of SWNTs [Raravikar-2002-235424]
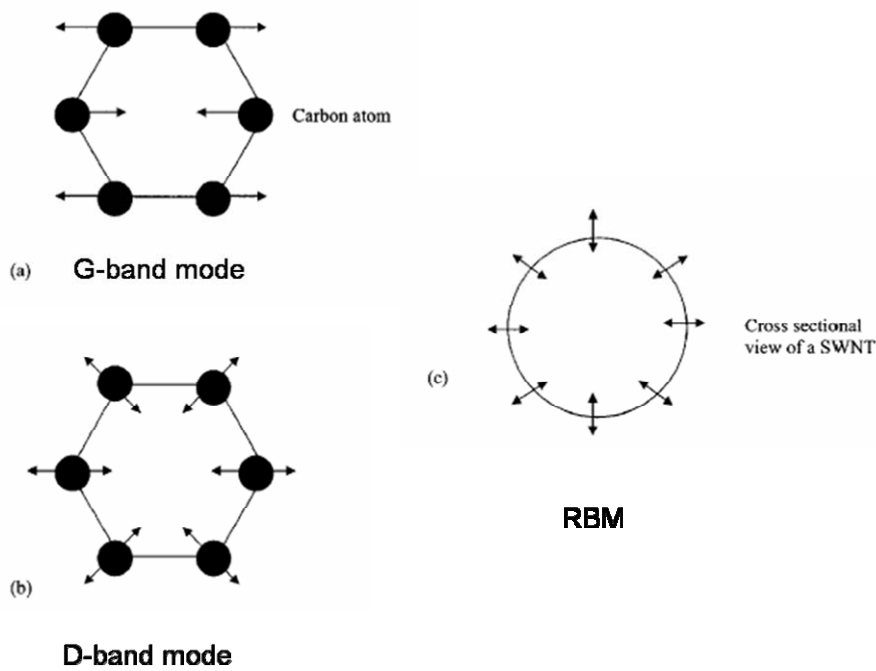
Fig. 2.24 Schematic diagram of Raman vibrational modes of CNTs (a) G-band mode (b)D-band mode (c)Radial breath mode [Raravikar-2002-235424]

(b) High-resolution transmission electron microscope (HRTEM) [Flahaut-2000-249]

HRTEM is the most direct method to analyze the structure of SWNT, however it is not easy to obtain a clear image of one SWNT. The main reasons are the structure of SWNT will be destroyed easily by high energy electron beam and electron scattering are not apparent because of SWNT is composed of so few carbon atoms. Furthermore, SWNT is hard to be built on stilts to avoid the background interference from copper grid and SWNTs dispersion are also an important problem. Figure 2.25 shows the HRTEM images of (a) SWNTs (b) SWNT bundles (c) DWNT (d) MWNT.
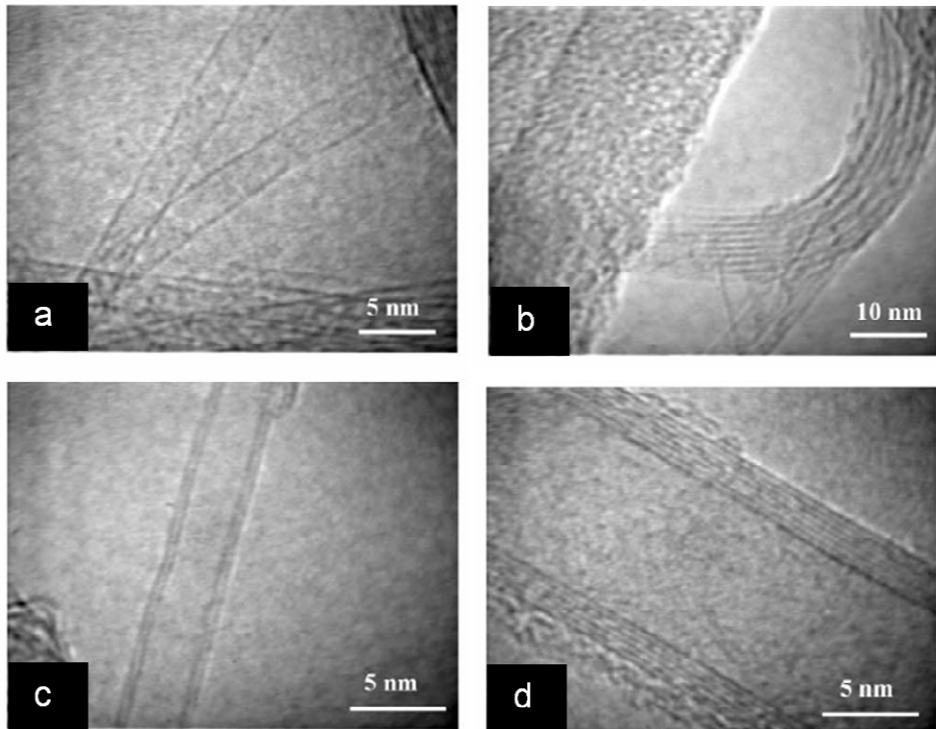
Fig. 2.25 (a) SWNTs (b) SWNT bundles (c) DWNT (d) MWNT [Flahaut-2000-249]
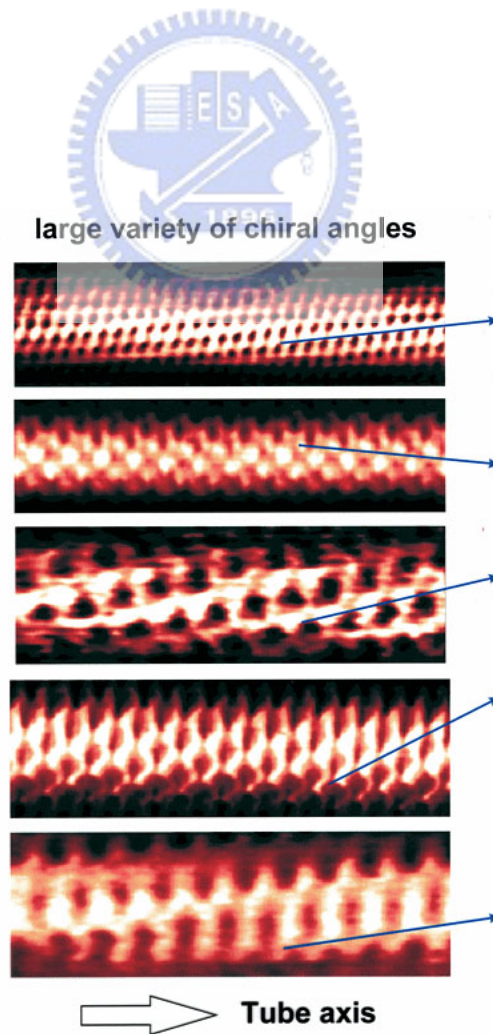
Fig. 2.26 STM image of various chiral angles SWNTs [Cees Dekker]

36

(c) Scanning tunneling microscope (STM)

STM can directly observe surface carbon atoms of SWNTs, providing information of carbon atoms site and arrangement. So we can measure length and chiral of SWNTs, as shown in Fig. 2.26.

2.6 Applications of SWNTs

Many researchers and engineers have been devoted to combine the CNTs with living. There are a lot of possible applications of CNTs products such as FED, field effect transistor (FET), hydrogen storage, etc. Until now, lots of prototypes of these applications have been published. Thus, it is believed that more and more commercial products will be published soon in the feature.

(a) Electron field emission elements:

The electron field emission elements, as implied by the name, utilized the field emission properties of CNTs. Among all of them, the closest to our life is FED. It is a next generation display after plasma display panel (PDP) and liquid crystal display (LCD) technologies. The theorem of formation of image is to use CNTs as cathode, then applies the potential between cathode and anode. Electrons emits from cathode to anode with phosphors which generate illumination. Ultra thin, wider view angle, superior brightness and low operation power are main advantages of FED. Samsung corporation had been public the

4.5" FED prototype in 1999 [Fig. 2.27].[Choi-1999-3129] And the electron source like SEM filament[Chow-1992-1] or X-ray tube[Yue-2002-355] can also employ the CNTs as electron emitters, which possess longer life, small energy spreading and power-saving significantly. Another field emission application related to general public is cathode-ray tube (CRT) lighting elements. The original has been published in 1998 by Ise Electronics corporation, Japan.[Saito-1998-L346] The fabricated CRTs are of a triode type, consisting of a cathode (nanotubes field emitter arrays), a grid and an anode (phosphor screen) [Figs. 2.28(a) and 2.28(b)]. The maxima brightness with anode at $200\,\mu$A is 64000 cd/cm^2. Stable electron emission, adequate luminance and long life (over 10000 hours) are demonstrated. It can be applied to a giant outdoor display or ultra-high quality color CRT displays.
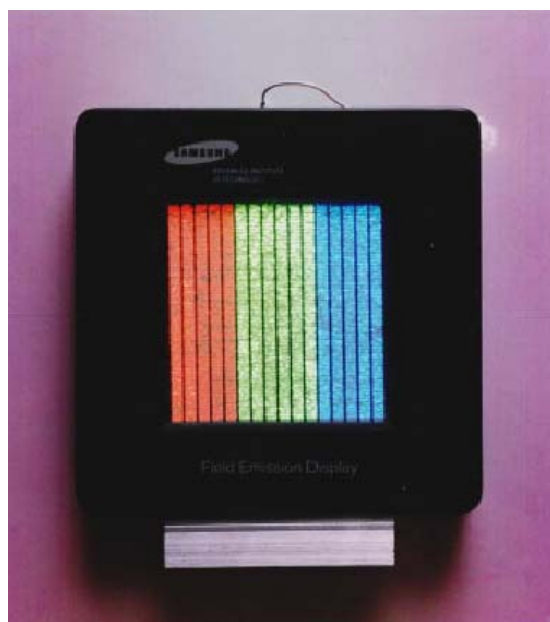
Fig. 2.27 FED display at color mode with red, green, and blue phosphor column.
[Choi-1999-3129]
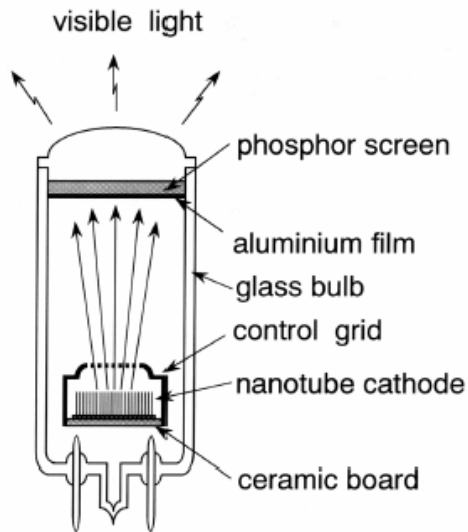
Fig. 2.28 Schematic drawing (a) and physical object (b) of a longitudinal cross section of a CRT fluorescent display with a field emission cathode composed of carbon nanotubes. [Saito-1998-L346]
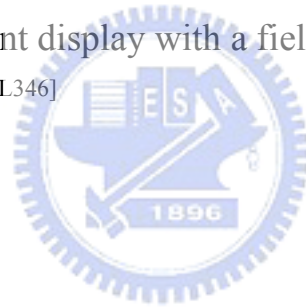
(b)FET

FET is a very important electronic device in history. The overwhelming majority of FET is silicon or Ⅲ－Ⅴ based just because these materials are semiconductors. But some of CNTs also have semiconducting properties, it makes researchers want to fabricate the CNTs based FET. In 1998, Sander reported the room-temperature transistor based on a single SWNTs FET. [Sander-1998-49] Fig. 2.29 shows the I-V curve of the CNT-FET. In 2001, Derycke in IBM corporation prepared both p-type and n-type nanotubes transistors to build the first nanotubes-based logic gates: voltage inverters [Figs. 2.30(a) and

2.30(b)]. [Derycke-2001-453] Surely, it still have lots of complicated problems to mass production above-mention devices, but these results have told that the nano-electronics is not hollow words any more.
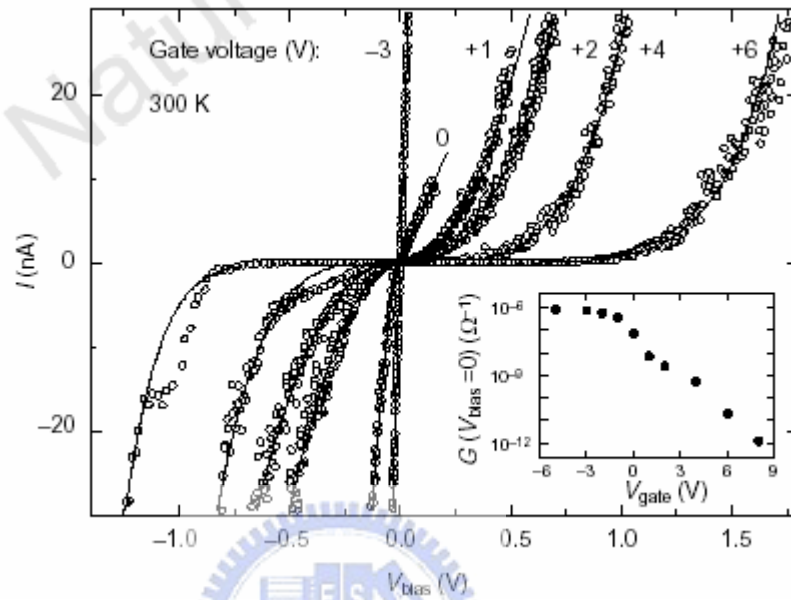
Fig. 2.29 Two probe I-V_{bias} curve for various values of the gate voltage from a CNTs-based FET. [Sander-1998-49]

(a)   (b)
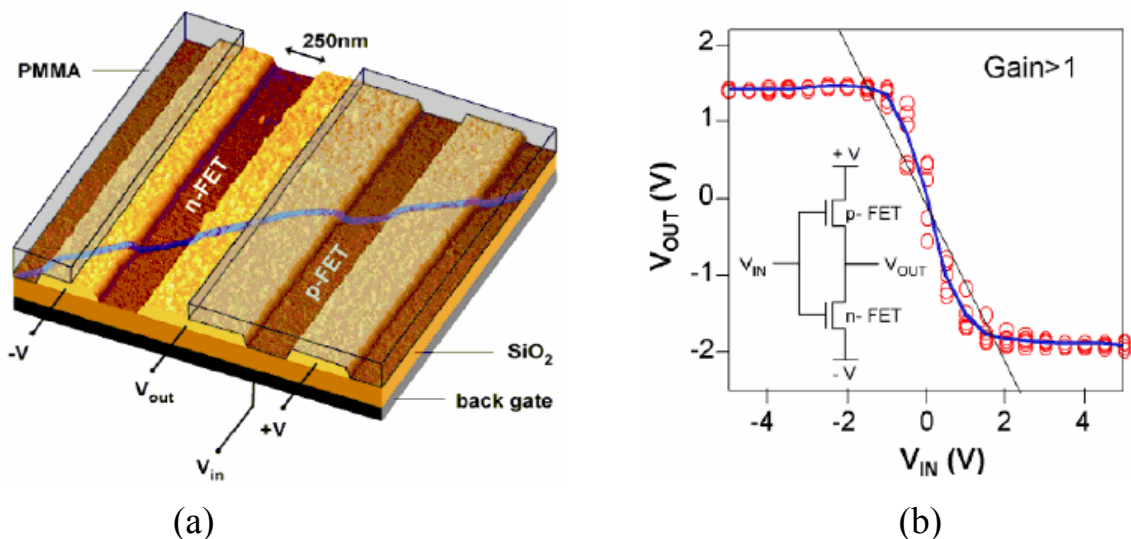
Fig. 2.30 (a) Atomic Force Microscopy (AFM) image shows the design of the voltage inverter. (b) Characteristics of the resulting intra-molecular voltage inverter. [Derycke-2001-453]

(c) Lithium intercalation

The basic principle of rechargeable lithium batteries is electrochemical intercalation and de-intercalation of Li in both electrodes. An ideal battery has a high-energy capacity, fast charging time and long cycle time. The capacity is determined by the Li saturation concentration of the electrode material. The SWNTs have shown to possess both high reversible and irreversible capacities [Gao-1999-153].

(d) Hydrogen storage material

Face to possible energy-crisis of gasoline, people has started to find the substitution methods for many years. Fuel cell was considered to have potential among all of solutions. Once it does be generated, its use as a fuel that creates neither air pollution nor greenhouse gas emissions. But it needs a huge hydrogen storage capability material. SWNTs just can play this role. SWNTs can absorb higher hydrogen than conventional materials. A H_2 uptake of 4.2 weight %, which corresponds to a H/C atom ratio of 0.52, was obtained by these SWNTs with an estimated purity of 50 weight %. Also, ~80% of the adsorbed H_2 can be released at room temperature. These results indicate that SWNTs are highly promising for H_2 adsorption even at room temperature [Liu-1999-1127]. The hydrogen storage mechanisms of CNTs are still not well known yet, and these properties usually occur at high pressure or low temperature environment. It remains

impossible to apply on commercial product so far.

(e) Composite materials

The SWNTs may be used as reinforcements in high strength, Low weight, and high performance composites due to their excellent mechanical properties. A main advantage of using SWNTs for structural polymer composites is that SWNT reinforcements will increase the toughness of the composites by absorbing energy during their highly flexible elastic behavior. Other advantages are the low density of the nanotubes, an increased electrical conduction and better performance during compressive load, or induced high thermal conductivity reinforced material.

(f) Other applications

Atomic Force Microscope (AFM) is employed to obtain the surface morphologies and roughness. It uses a probe scanning the surface of sample, and an incident laser beam irradiates the arm of probe reflecting to a detector which passes signals to computer and draws the images. In order to obtain a high resolution images, the tip must be ultra thin, extremely sharp and high strength. General type of AFM tip is made of Si_3N_4. The first article that utilized SWNTs as AFM tip was reported in 1996[Fig. 2.31]. [Dai-1996-147] From Fig. 2.32, one can clearly see the SWNTs tip shows the better image resolution. At the same time, SWNTs with excellent mechanical properties can make the damage ratio of tip

decrease as low as possible. It has been some commercial products of SWNTs

AFM tip at present.

In 1998, Wong demonstrated that CNTs tip can be used for chemical and

biological discrimination.[Wong-1998-52] Another possible application applied to

biotechnology of medicine carriers are developing as well. In the feature, people

will easily get to know what disease that we get. Also, people can use CNTs

filled with drags injecting into body, then induce it to the proper position

relaxing the medicine to destroy the etiology without hurting normal cell nearby.
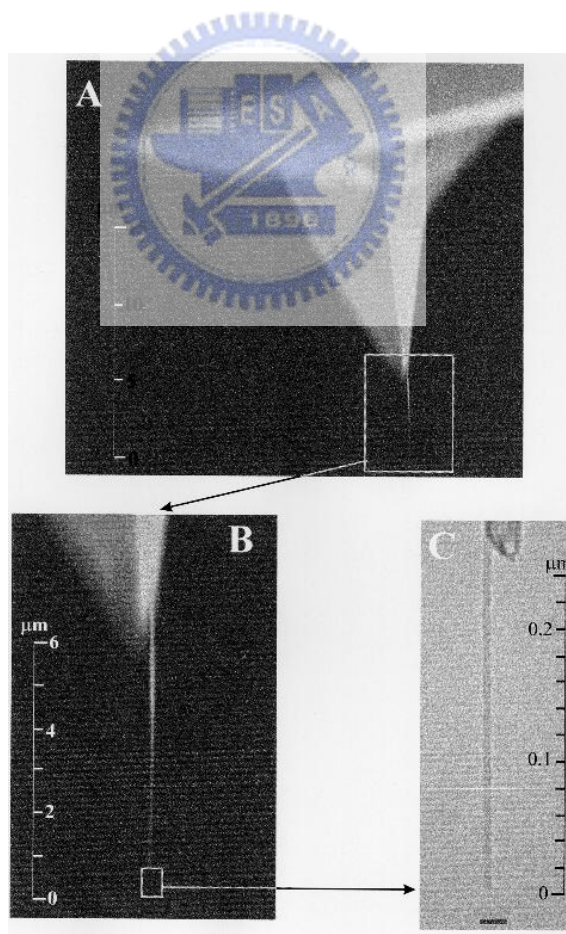
Fig. 2.31 SWNT attached to the pyramidal tip of a silicon cantilever for AFM.
[Dai-1996-147]
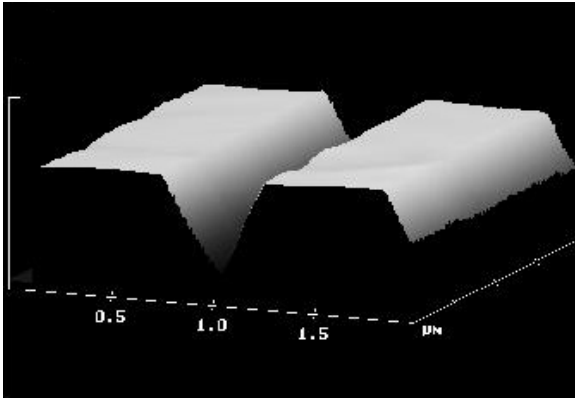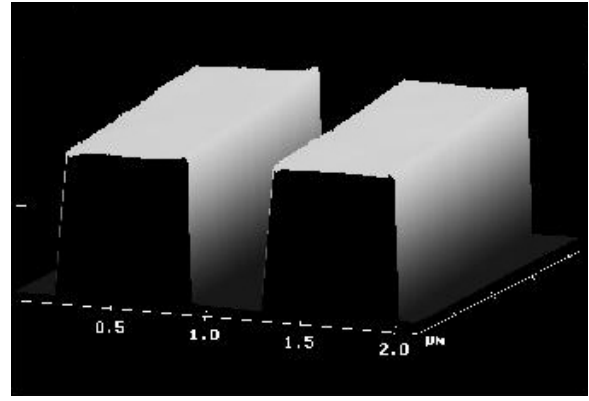
(a)   (b)

Fig. 2.32 (a)Tapping mode AFM image of a 400-nm-wide, 800-nm-deep trench taken with a bare pyramidal tip. (b) The image taken with a nanotubes attached to the pyramidal tip with the same specimen.[Dai-1996-147]

Chapter III
Experimental Methods

3.1 Flow chart
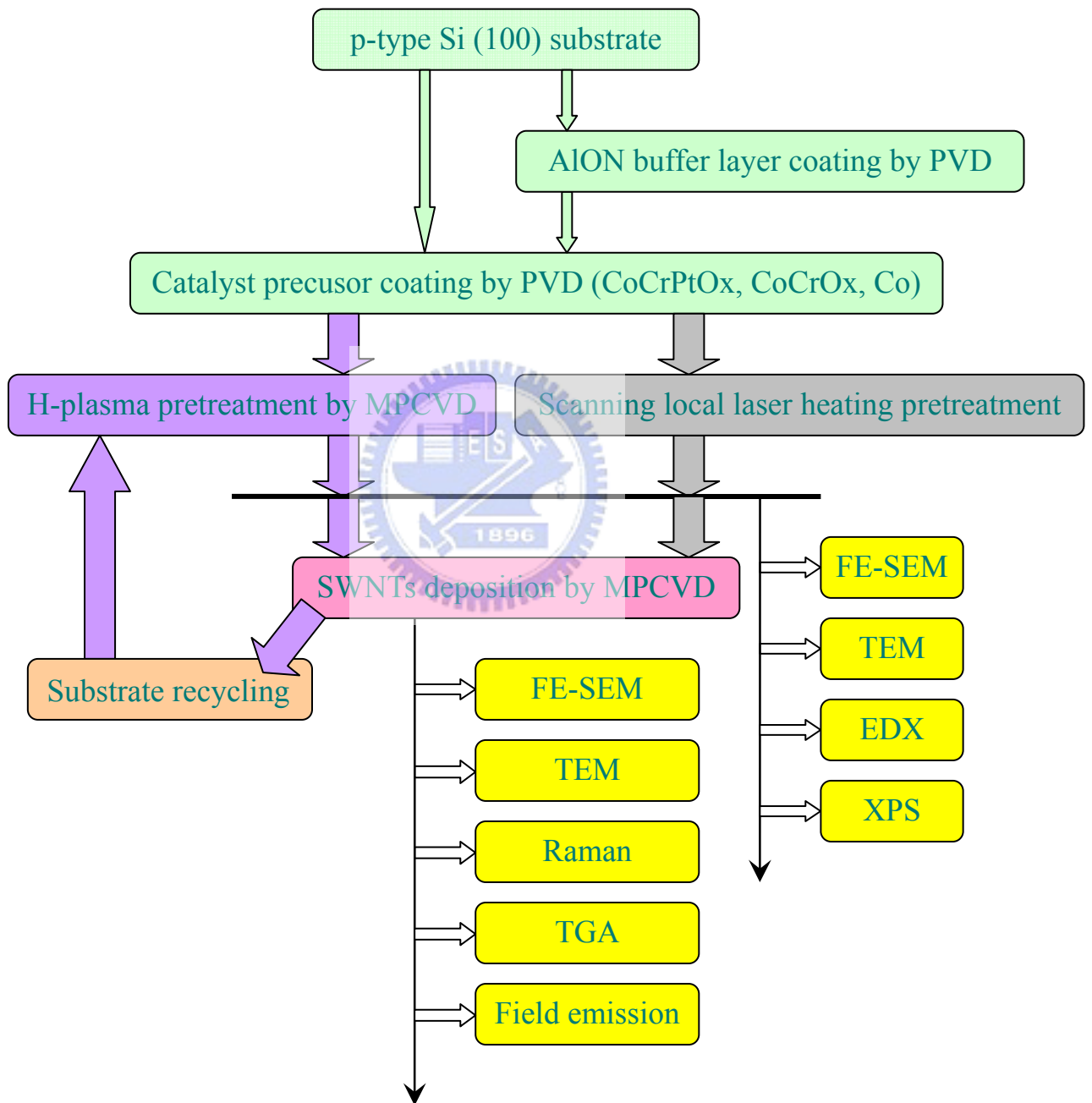
Fig. 3.1 Flow Chart of the experiment

Figure 3.1 shows the experimental flowchart for the fabrication and analyses of the catalyst precursor-assisted SWNTs. First, the $CoCrPtO_x$ films to act as catalyst precursor were deposited by physical vapor deposition (PVD) and buffer layers were prepared by DC reactive sputter. Then, two type of pretreatment were used. (1) H-plasma pretreatment was performed in microwave plasma chemical vapor deposition (MP-CVD) system to carry out reduction of oxidized $CoCrPtO_x$ film on silicon wafer. The specimens were subsequently heated up to grow SWNTs in an appropriate CH_4/H_2 atmospheres for several minutes at appropriate chamber pressure. (2) Local laser heating pretreatment was operated using 659 nm pump laser to heat numerous spots on substrate surface up to ~700 ^oC, and then transferred specimens to MPCVD chamber to synthesize SWNTs on Si substrate. The morphologies of the pretreated catalyst precursor were studied by scanning electron microscopy (SEM). The size and distribution conditions of catalyst particles after pretreatment on the silicon wafer were characterized from grinding cross-section and plane view samples by transition electron microscopy (TEM). Additionally, X-ray photoelectron spectroscopy (XPS) was employed to characterize binding energy of $CoCrPtO_x$ layer at as-deposited and after H-plasma pretreatment to analyze the self-assembly mechanism. The morphologies, microstructures and bonding structures of the as-grown SWNTs were investigated by SEM, TEM and Raman

spectroscopy with a 632.8 nm He-Ne laser, etc. The field emission measurements (*J-E*) of the specimens were conducted by the simple diode configuration and performed in high vacuum. The oxidation resistance properties of as-grown SWNTs was measured by thermal gravimetric analysis (TGA).

3.2 Raw materials

(a) Substrates:

    Silicon wafer   [P-type (100)]

(b) Source gases:

    Hydrogen gas   (purity 99.9995%)   Jian Ren Chemical Co.

    Methane gas   (purity 99.999%)   San Fu Chemical Co.

    Oxygen gas   (purity 99.9995%)   Jian Ren Chemical Co.

    Nitrogen gas   (purity 99.998%)   Jian Ren Chemical Co.

    Argon gas   (purity 99.9995%)   San Fu Chemical Co.

(c) Target:

    CoCrPt   Co 57.08 %, Cr 10.97 %, Pt 31.95 %

    CoCr   Co 67.19%, Cr 32.81%

    Al   purity 99.999%

3.3 Strategy of self-assembly CoCrPtO$_x$ catalyst precursor

As shown in Fig. 2.12, the oxidized phase of PtO$_x$ is unstable and can be easily reduced back to metallic state with very fine size when temperature is approximately 500 °C [Kim-2003-1701]. Hence, it has been recently used in optical storage media and nonvolatile memory, as shown in section 2.2. Additionally, Co is the good element for carbon species dissolubility and Cr$_2$O$_3$ are revealed to suppress the grain growth of Ni-Cr alloy effectively [Shaijmon-2005-192]. Combining these unique properties, oxidized film of CoCrPt deposited by PVD is acted as the catalyst precursor to fabricate vertically well-aligned SWNTs and synthesize SWNTs with low process temperature on Si substrate in this study.

3.4 Catalyst precursor and buffer layer deposition procedures

(a) Catalyst precursor

The CoCrPtO$_x$ thin films which were as catalysts were coated on a (100)-oriented *p*-silicon wafer with and without buffer layer using a pure CoCrPt target by PVD (Helix 6-gun) in a mixed argon and oxygen atmosphere. The argon and oxygen ratio for depositing was 10:30 (sccm/sccm) and the deposited thickness of CoCrPtO$_x$ films were 1, 2, 3, 5, 10 nm.

(b) Buffer layer

AlON which was reported as the most efficient buffer layer [Wang-2005-1906]

was used in this study. AlON film was deposited on a (100)-oriented *p*-silicon wafer by DC reactive sputtering (Unaxis Cube Trio) using an Al target in a gas mixture of oxygen, nitrogen and argon. The deposited thickness of AlON film was 10 nm which was the best thickness to assist catalyst particles in distributing, as shown in section 2.2[Wang-2005-1906].

3.5 Microwave plasma chemical vapor deposition system (MPCVD)

The schematic diagram of MPCVD system is shown in Fig. 3.2. The main components of the system can be divided into six parts: the microwave generator, wave guides, reaction chamber, gas flow controller, gas pressure controller and pumping system. The microwave generator of microwave source system (Frequency 2.45 GHz, Power 1.3 kW) was produced by Tokyo electronic Corp. Ltd. The reaction chamber contains quartz tube (inner: 47 mm, outer: 50 mm, China Quartz Corp. Ltd), stainless chamber, stainless holder and rotary pump (Hitachi Corp. Ltd). As Fig. 3.3 shown, sample holder is manufactured by stainless steel, it can bear high working temperature and reduce vacuum pollutions while plasma working. The upper electrode that was made by stainless steel is connected to the DC power supply output. The upper electrode (ground) and substrate holder (negative) were employed to applying the substrate negative bias. The substrate temperature is measured by thermal couple

which equipped in the holder. Mass flow control (MKS model 247) system is used to regulate the flow rate of reacting gas while depositing. Besides, the flow rate controller with different range (1-10 sccm, 10-100 sccm) of flow rate of mass flow control system can be properly adjusted for different gas (Ar, NH_3, H_2, CH_4, C_2H_2). The low pressure (0.1~100 Torr) of chamber can be detected by thermal couple of vacuum gauge and absolute pressure gauge (MKS Baratron). The work pressure of chamber can be regulated stably by throttling valve. The degree of the throttling valve was controlled by APC controller (MKS model 263). There is no external heater system equipped on MPCVD. The plasma is used to heat the substrate as the heat source. Cooling cycle system is made up of the refrigerator with closed cooling water and the conduit.
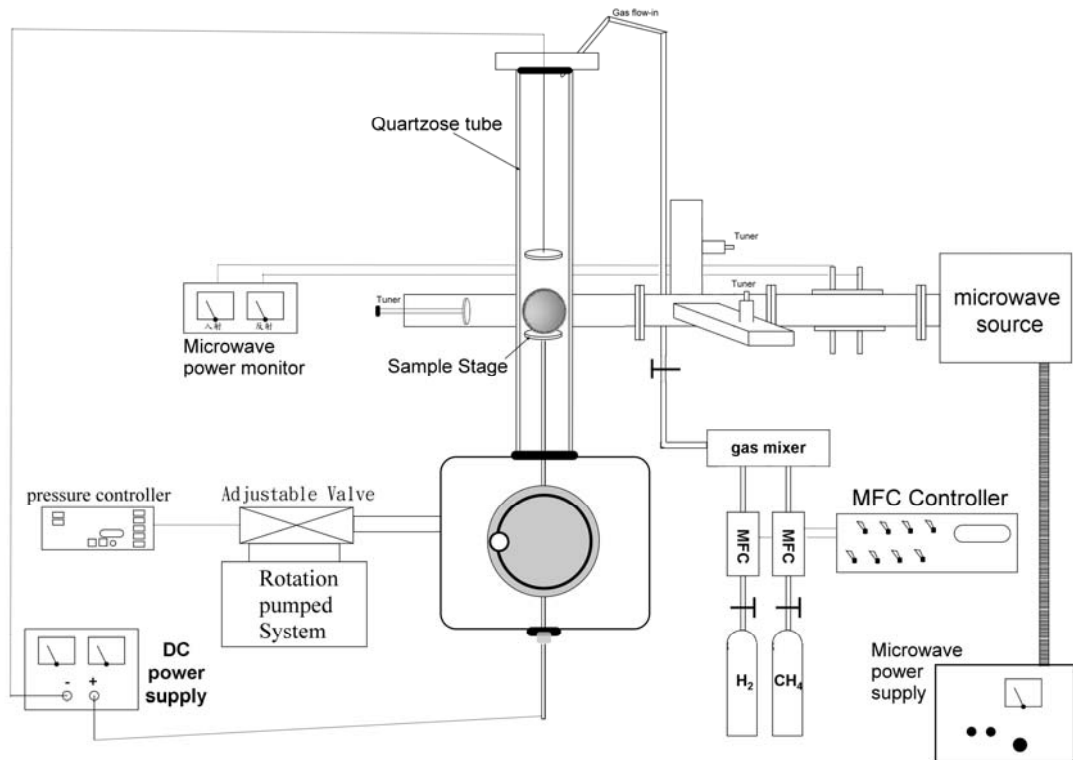
Fig. 3.2 Schematic drawing of MPCVD system
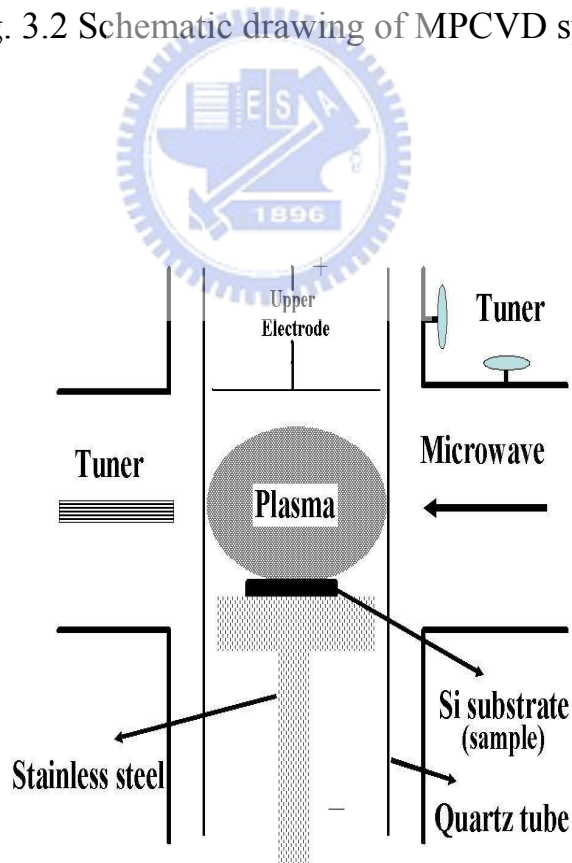
Fig. 3.3 Schematic drawing of MPCVD reactor

3.6 Pretreatment methods

3.6.1 H-plasma pretreatment by MPCVD

After catalyst precursor and buffer layer deposition, the specimen was transferred in air to the chamber of MPCVD which was pumped down to its base pressure. Hydrogen plasma was utilized to activate the $CoCrPtO_x$ film and change surface morphology of it. The purpose of this part is to find out the optimum conditions of H-plasma pretreatment to obtain the small average size distribution and appropriate density of catalyst nano-particles. The most optimum $CoCrPtO_x$ catalyst precursor pretreatment conditions were: microwave power 600 W, working pressure 30 Torr, sample temperature 580 ^{o}C, H_2 flow 100 sccm and process time 10 minutes. Finally, we draw three straight lines on SEM micrograph and calculate the average particle size by the ratio of line length to particle numbers.

3.6.2 Scanning local laser heating pretreatment

For scanning local laser heating pretreatment, catalyst precursor-deposited sample was transferred to the chamber of two laser static tester (Tueopicts, 633-nm-wavelength cw model diode laser and 659-nm-wavelenth duration mode diode laser). The 633-nm laser was used to monitor the reflectivity change to focus another 659-nm laser. Then using 659-nm pump-laser to heat numerous spots on substrate surface simultaneously to carry out reduction of oxidized

CoCrPtO$_x$ film up to ~ 700 ^{o}C and then well-distributed fine nano-particles were formed on transparent or Si substrate. Figure 3.4 shows the schematic diagram of local laser heating pretreatment. The most optimum local laser heating pretreatment conditions were: laser peak power 3 mW, process time 20 ns.
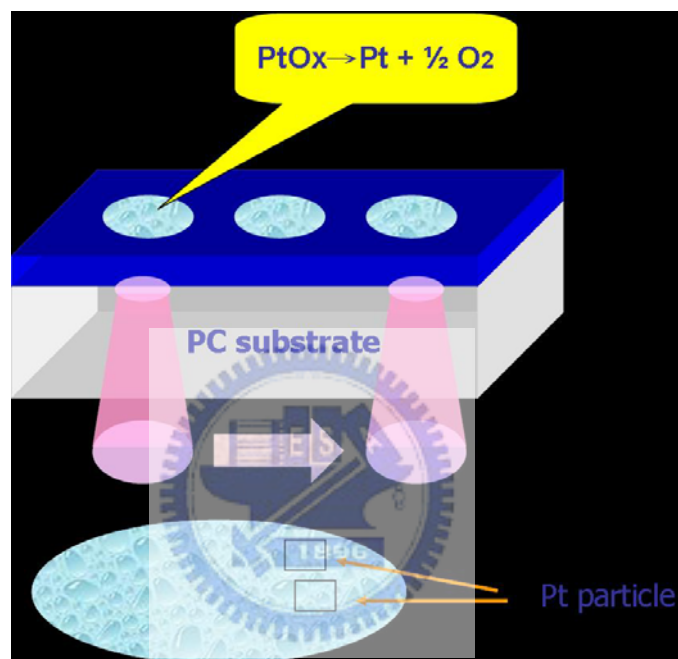
Fig. 3.4 Schematic drawing of scanning local laser heating pretreatment

3.7 Specimen stacking methods and growth procedures of SWNTs

Design of specimen stacking sequences

The important parameters of carbon nanostructure growth procedures are gas ratio, gases flow rate, microwave power, working pressure, sample temperature, process time and specimen stacking sequences, etc. These parameters may affect the morphology, uniformity, quality of the SWNTs. The

specimen stacking sequences were shown in Fig. 3.5. Four the same specimens are placed one time. Sample A is placed upside down to face sample B upside. Sample C is placed backside to face sample D upside.

Two experiments are studied as follows:

(a) Synthesize high quality well-aligned SWNTs (H-plasma pretreatment):

Due to high quality and high aspect ratio SWNTs can enhance electrical properties, thermal conductivity, mechanical properties and field emission properties, thus H-plasma pretreatment and buffer materials were utilized to approach this target. H-plasma pretreatment can etch catalyst film to become the finest nano-particles with uniform size and buffer layer can make nano-particles distribute uniformly and densely. Moreover, reduction reaction of oxidized $CoCrPtO_x$ film can form well-distributed fine nano-particles on silicon wafer. Thus, high quality well-aligned SWNTs can be synthesized by MPCVD. The optimum deposition conditions for the SWNTs growth were: microwave power 750 W, working pressure 24 Torr, sample temperature 600 ^{o}C, H_2/CH_4 ratio = 50/4 (sccm), and deposition time 1~6 minutes for length control.

(b) Low temperature synthesis of SWNTs (Laser ablation pretreatment):

SWNTs have recently been considered as a promising candidate material for application as field emitters, nano-electronic devices (e.g., single electron transistor), et al. For such applications, the deposition temperature must be

lowered, particularly for compatibility with IC processes, and structural manipulation becomes an important issue. Therefore, in order to fabricate SWNTs with desired morphology at low temperatures, laser ablation pretreatment was utilized. Laser can heat a number of spots on substrate surface up to 700 $^{\circ}$C in nano-seconds, and then sink heat rapidly to whole sample. From this, transparent PC substrate won't be damaged, and PtO$_x$ can be reduced to nano-particles. Thus, SWNTs can be synthesized on transparent PC substrate by MPCVD at low temperature. The optimum deposition conditions for the SWNTs growth were: microwave power 300 W, working pressure 11 Torr, sample temperature 373 $^{\circ}$C, H$_2$/CH$_4$ ratio = 50/4 (sccm), and deposition time 1~4 minutes for length control.
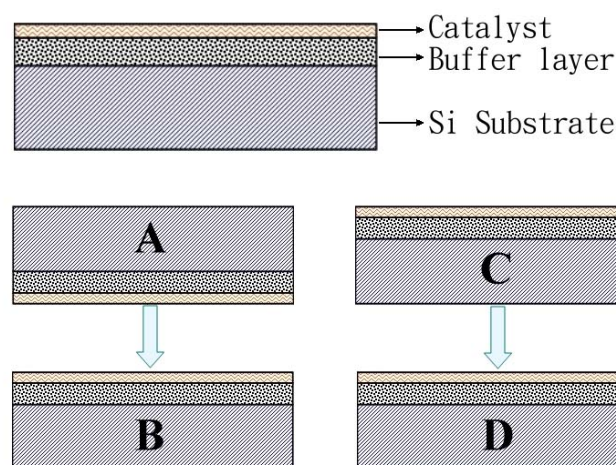
Fig. 3.5 Schematic diagram of specimen stacking sequences

Substrate recycling:

Substrate recycling process was studied by removing the as-deposited nanostructures from the substrates in ultrasonic bath, and the substrates were then pretreated in H-plasma to reactivate the catalyst particles on the substrate. The well-aligned SWNTs can be obtained by substrate recycling for several times using the same procedures and conditions described in section 3.7(a).

Our specimen designation is shown in Table 3.1.

Table 3.1 Specimen designation and pretreatment and growth conditions

Specimen designation	Catalyst precursor thickness (nm)	Buffer layer thickness (nm)	Pretreatment	Growth method
A1	10 nm $CoCrPtO_x$		HP	MPCVD - H
A2	5 nm $CoCrPtO_x$		HP	MPCVD - H
A3	3 nm $CoCrPtO_x$		HP	MPCVD - H
A4	2 nm $CoCrPtO_x$		HP	MPCVD - H
A5	1 nm $CoCrPtO_x$		HP	MPCVD - H
A6	1 nm $CoCrPtO_x$	10 nm AlON	HP	MPCVD - H
B1	5 nm Co		HP	MPCVD - H
B2	5 nm $CoCrO_x$		HP	MPCVD - H
B3	5 nm $CoCrPtO_x$		HP	MPCVD - H
C	1 nm $CoCrPtO_x$		SP	MPCVD - L

HP: H-plasma pretreatment, microwave power 600 W, working pressure 30 Torr , sample temperature 580°C, H_2 flow 100 sccm, process time 10 minute.

SP: Scanning local laser heating pretreatment, laser peak power 3 mW, process time 20 ns.

MPCVD - H: Microwave power 750 W, working pressure 24 Torr. sample temperature 600°C, H_2/CH_4 ratio = 50/4 (sccm/sccm), deposition time 6 minutes.

MPCVD - L: Microwave power 300 W, working pressure 11 Torr, sample temperature 373 °C, H_2/CH_4 ratio = 50/4 (sccm/sccm), deposition time 4 minutes.

3.8 Structure analyses

3.8.1 Scanning electron microscopy (SEM)

SEM is a very useful tool for observing surface morphology of specimen. SEM has secondary electrons (SE) or backscattered electrons (BSE) detectors passing the signal to computer and forming image. In this study, the surface morphology of as-pretreated catalyst precursor and SWNTs were characterized by focused ion beam & electron beam (FIB/SEM) system. The cross-section view of as-grown SWNTs was investigated by field-emission SEM (FE-SEM) (JEOL 6300) operating at 15 kV accelerating voltage.

3.8.2 Transmission electron microscopy (TEM)

The TEM image is the result of electron transmitting through the sample, and it reveals the interior microstructure of the specimen, and it can give the high-resolution lattice image and the electron diffraction pattern as well. In the experimental, the microstructure of as-grown SWNTs were characterized by JEOL, JEM-2010F TEM operating at 200 kV accelerating voltage. The size and distribution conditions of catalyst nano-particles after pretreatment on the silicon wafer were characterized from grinding cross-section and plane view samples by Philips, TECNAI 20 TEM/EDX. TEM cross-sectional specimens for the TEM analyses were prepared by mechanical polishing and subsequent argon ion

milling.

3.8.3 Raman spectroscopy (Raman)

Raman scattering was discovered by Raman in 1928. If an incident photon occurs inelastic scatter with specimen molecules and causes the energy change of the photon called Raman scattering. By this mechanism, one can measure the difference between incident and scattering light by a spectrometer to obtain the information of element and bonding structure of the specimen. In particular, Raman spectroscopy is useful in identifying carbon-based materials. There are two obvious bands located at about 1330 cm^{-1} (D band) and 1590 cm^{-1} (G band) which correlate with the vibration of sp^3-bonded and sp^2-bonded carbon atoms, respectively. Additionally, the special radial breathe mode (RBM) is a unique feature in the Raman spectrum of SWNTs and involves a collective vibrational movement of the carbon atoms towards and away from the central axis of a SWNT. Consequently, the associated RBM Wavelength and frequency are directly related to the perimeter of the nanotube. Base on this relationship, as the diameter of the nanotube increases, the RBM frequency shifts to lower wave numbers, as shown in section 2-5. In order to study the structural characterization of the SWNT samples, a Jobin Yvon LABRAM HR Micro-Raman system with a He-Ne laser (wavelength: 632.8 nm) was utilized in

the experiments.

3.8.4 X-ray photoelectron spectroscopy (XPS)

Surface analysis by XPS involves irradiating a solid in vacuum with mono-energetic soft X-rays and analyzing the emitted electrons by energy. The spectrum is obtained as a plot of the number of detected electrons per energy interval versus their kinetic energy. Quantitative data can be obtained from peak height or peak areas, and identification of chemical states often can be made from exact measurement of peak positions and separations. In this study, XPS was employed to characterize binding energy and chemical state of the of the ultra-thin $CoCrPtO_x$ layer at as-deposited and after H-plasma pretreatment to analyze the self-assembly mechanism. XPS analyses were performed on ESCA system (VG Scientific, Microlab 350) with Al-$K\alpha$ (1486.6 eV) excitation. X-ray emission energy was 400 W with 15 kV accelerating voltage. Argon ion with ion energy of 5 keV was used for sputter profiling.

3.8.5 Energy-dispersive X-Ray analyses (EDX)

EDX Analysis stands for Energy Dispersive X-ray analysis. It is sometimes referred to also as EDS or EDAX analysis. It is a technique used for identifying the elemental composition of the specimen, or an area of interest thereof.   The

EDX analysis system works as an integrated feature of SEM or TEM, and can not operate on its own without the latter. In the experimental, the elemental composition of catalyst was characterized by Philips, TECNAI 20 TEM/EDX.

3.9 Properties analyses

3.9.1 Field emission measurements (*J-E*)

In section 2.1, the field emission properties of SWNTs have been described. The measurements were conducted by the simple diode configuration and carried out in a high vacuum chamber pumped down to a pressure of about 10^{-6} Torr with a turbo molecular pump, backed up by a rotary mechanical pump. Figure 3.6 shows the instrument setup and the test configuration used during field emission characterization. A steel probe with a diameter of 1.8 mm as anode was used for the measurement. The distance between the specimen and anode was about 100 μm controlled by a precision screw meter, and effective field emission area of the specimen was 0.025 cm^2. The specimen (cathode) was biased with a voltage swept positively from 0 to 1000 V at room temperature to extract electrons from emitters. A high voltage source-measure unit (Keithley 237) was used for providing the sweeping electric field (*E*) and monitoring the emission current density (*J*). The measurement instruments are auto-controlled by the computer. Prior to the field emission measurement, a high constant

voltage of about 600 V was applied to the emitters to exhaust the adsorbed molecules.
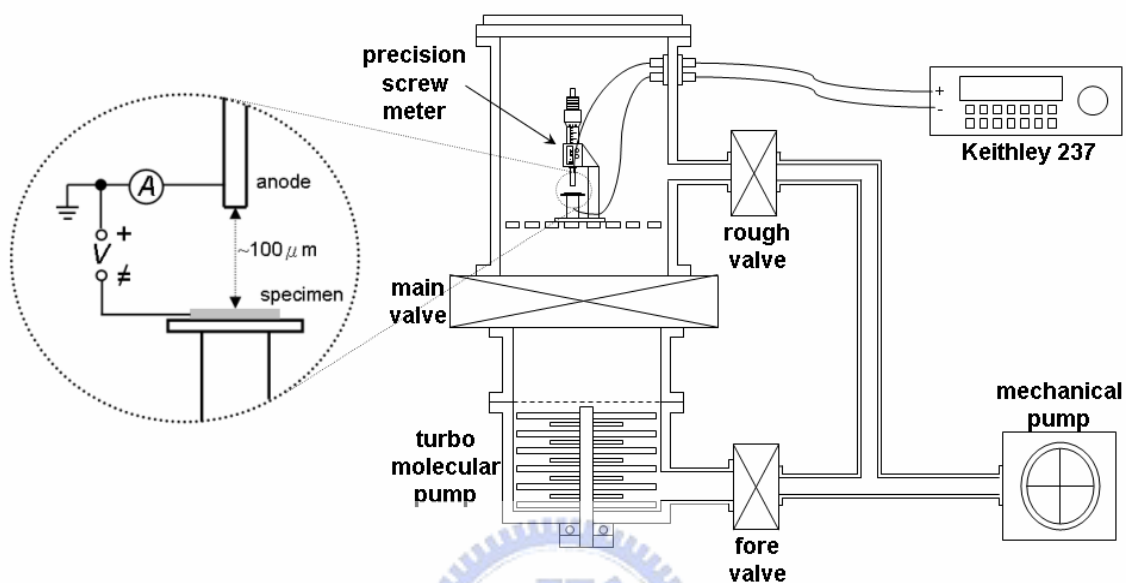
Fig. 3.6 Schematic diagram of the field emission measurement setup

3.9.2 Thermal gravimetric analysis (TGA)

In a Thermo gravimetric analysis, the percent weight loss of a test sample is recorded while the sample is being heated at a uniform rate in an appropriate environment. The loss in weight over specific temperature ranges provides an indication of the composition of the sample, including volatiles and inert filler, as well as indications of thermal stability. Set the inert (usually N_2) and oxidative (O_2) gas flow rates to provide the appropriate environments for the test. In this experiment, Shimadzu TGA-50 was implemented on 5 mg of the as-grown SWNTs. We used razor blade to remove the as-grown SWNTs from

the substrate and collect 5-mg SWNTs sample to place in the alumina cell. Set

the initial weight reading to 100%, and then initiate the heating program with 10

°C/min ramp rate. The gas environment is an oxidative decomposition (air, 30

sccm/min).

Chapter **IV**
Results and discussions

4.1 Microstructures and XPS spectra of the H-plasma-pretreated catalysts

4.1.1 Effect of catalyst precursor thickness and buffer layer

Figure 4.1 illustrates the typical SEM morphologies of the pretreated catalyst precursor on silicon wafer without application of buffer layer and with various $CoCrPtO_x$ catalyst precursor thicknesses: (a) 10 nm, (b) 5 nm, (c) 3 nm, (d) 2 nm, (e) 1 nm and (f) 1 nm, respectively, except Fig. 4.1(f) is the catalyst precursor morphology with 10 nm AlON as buffer layer. It indicates that the average catalyst size after pretreatment is smaller for the smaller catalyst precursor thickness, as also shown in Table 4.1. By comparing the same catalyst precursor thickness but with and without buffer layer application in Table 4.1, the specimen with buffer layer gives rise to a smaller particle size.

It is believed that very fine, dense and uniformly distributed catalyst particles after H-plasma pre-treatment can give rise to growth of the vertically and well aligned tubes due to mutual restriction between tubes. In contrast, the scarce particle distribution may result in growth of spaghetti-like CNTs. To examine this possibility, top-view and cross-sectional HRTEM micrographs of the H-plasma pre-treated catalysts without buffer layer are shown in Figs. 4.2(a)
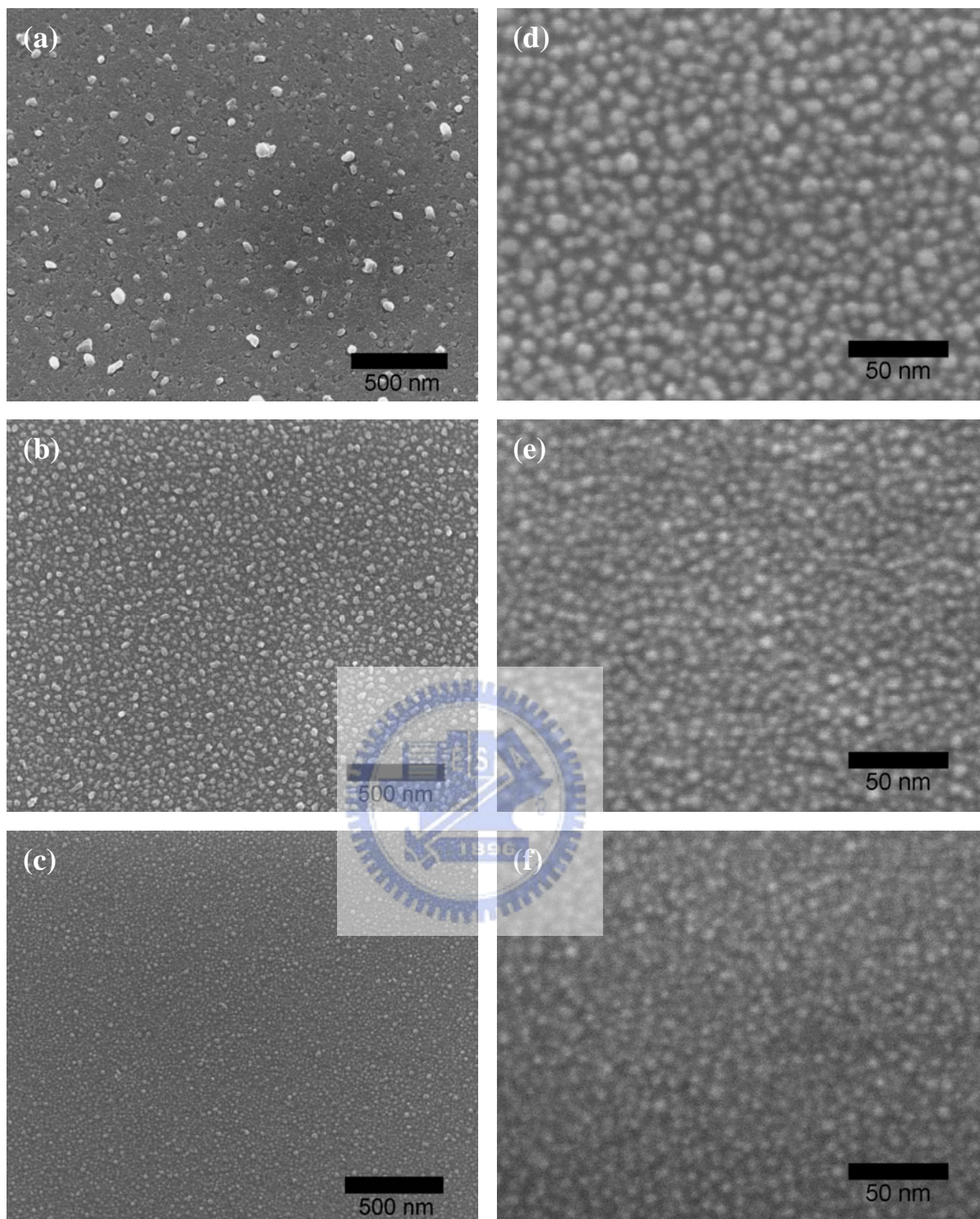
Fig. 4.1 Top-view SEM images of the pretreated catalyst precursor on silicon wafer without application of buffer layer and with various $CoCrPtO_x$ catalyst precursor thicknesses: (a) 10 nm, (b) 5 nm, (c) 3 nm, (d) 2 nm, (e) 1 nm and (f) 1 nm, respectively, except Fig. 4.1(f) is the catalyst precursor morphology with 10 nm AlON as buffer layer.

Table 4.1 CoCrPtO$_x$ film thickness versus H-plasma pretreated average particle size.

Specimen designation	Film thickness (nm)	Average particle diameter from SEM figure (nm)[1]	Corresponding SEM figure	Particle size from TEM
A1	10	57.8	4.1(a)	
A2	5	22.6	4.1(b)	
A3	3	8.3	4.1(c)	
A4	2	6.1	4.1(d)	
A5	1	3.2	4.1(e)	3.5
A6	1 [2]	2.3	4.1(f)	2.4

[1] H-plasma pretreatment conditions: microwave power = 600 W, H$_2$ = 100 sccm, working pressure = 30 Torr, process time = 10 min, temperature = 580 °C.

[2] For Si substrate with 10 nm AlON buffer layer.

and 4.2(b), respectively. It shows uniform distributed nano-particles with diameters ranging from 3 nm to 4 nm with an average value of 3.5 nm, which is quite close to 3.2 nm from SEM examinations in Fig. 4.1, as also shown in Table 4.1. Effect of buffer layer on the H-plasma pretreated catalyst formation is demonstrated in Figs. 4.2(b) and 4.2(c), where the catalyst precursor-coated substrates have the same thickness, but without and with AlON buffer layer, respectively. The corresponding EDX spectra for the H-plasma-pretreated catalyst precursors in Figs. 4.2(b) and 4.2(c) are shown in Figs. 4.3(a) and 4.3(b), respectively, indicating existence of buffer layer after pretreatment. It appears that the particle sizes after H-plasma pretreatment for the substrate with buffer layer are ranging from 1 ~ 3 nm (average 2.4 nm), which is smaller than the
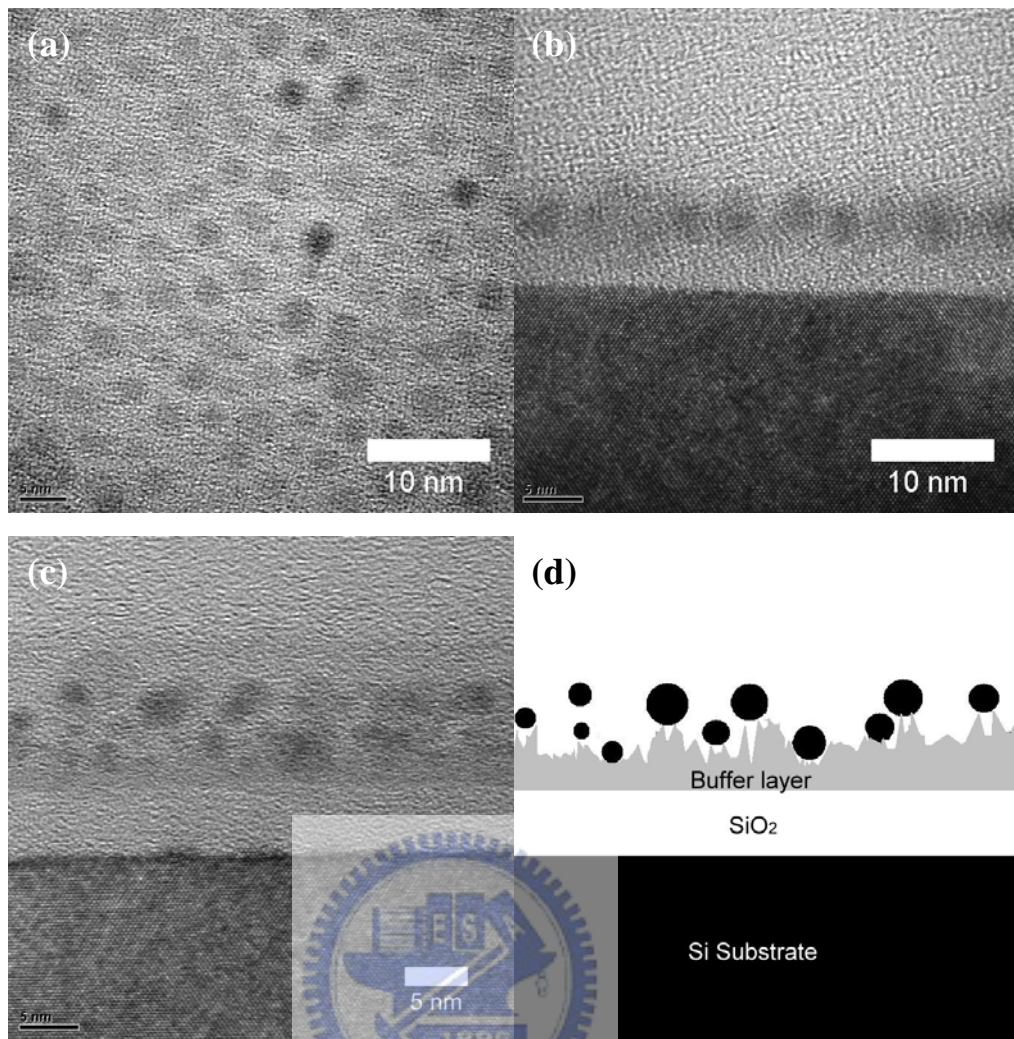
Fig. 4.2 HRTEM micrographs: (a) Top-view and (b) cross-section of pretreated 1 nm catalyst precursor without buffer layer. (c) Cross-section of pretreated 1 nm catalyst precursor with buffer layer. (d) Schematic diagram of Fig. 4.2(c).

corresponding value (average 3.5 nm) in Fig. 4.2(b). Effect of buffer layer is essentially to minimize the nano particle aggregation during H-plasma pretreatment. This is concluded from the cross-sectional view of Figs. 4.2(b) and 4.2(c), where the nano-particles seem to be trapped in the valleys of the surface, as schematically shown in Fig. 4.2(d).   In additional to a buffer layer in Fig. 4.2(c), both Figs. 4.2(b) and 4.2(c) indicate formation of SiO_2 layer (~ 4 nm)

after pretreatment, which is formed in the earlier stage of the pretreatment and may act as buffer layer effect in Fig. 4.2(b).

Element	Weight %	Atomic %
O K	59.1	88.0
CrK	0.9	0.4
CoK	23.7	9.6
PtL	16.3	2.0
Total	100.0	100.0

Element Net Inte. Backgrd Inte. Error P/B

(a)   **(b)**
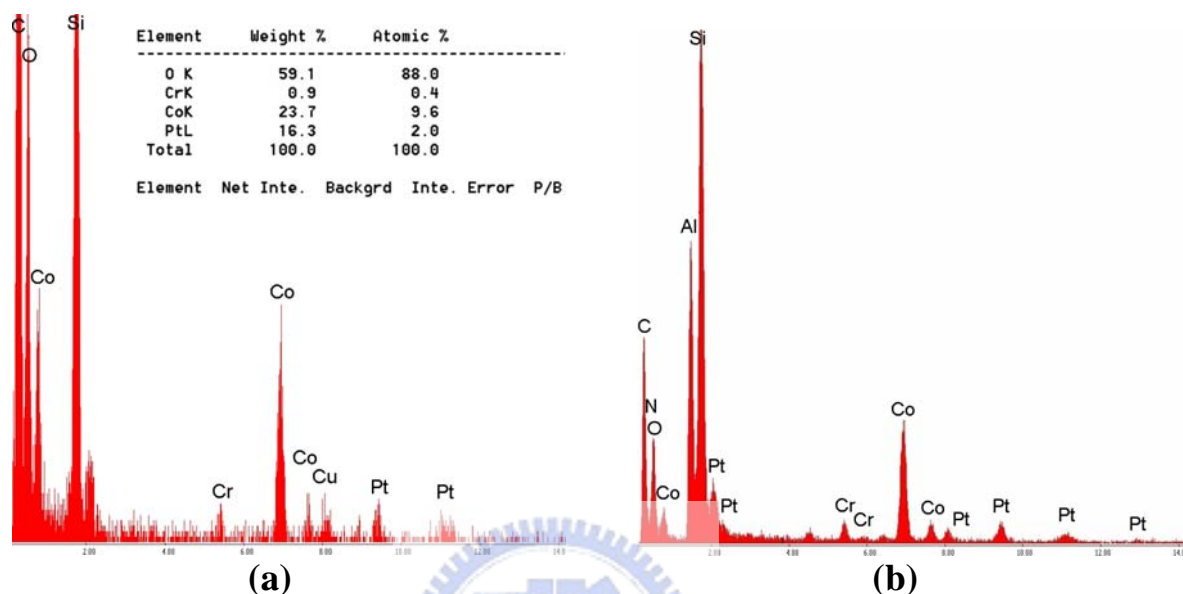
Fig. 4.3 EDX spectra of the H-plasma pretreated catalyst precursors on Si substrates: (a) 1 nm catalyst precursor without buffer layer and (b) with buffer layer.

4.1.2 Effect of catalyst precursor oxygen content

Effect of oxygen contents of CoCrPt films is displayed by SEM micrographs in Figs. 4.4(a) to 4.4(d) for the H-plasma pretreated catalyst precursors, where the catalyst precursors of 10 nm thickness in Figs. 4.4(a) and 4.4(c) were coated on the substrate under Ar + O_2 atmosphere (Ar:O_2 = 10:30 sccm/sccm); and under pure Ar atmosphere (40 sccm) for catalyst precursors in Figs. 4.4(b) and 4.4(d).   The catalysts in Figs. 4.4(a) and 4.4(b) were H-plasma pretreated at 515°C for 8 min; and at 591°C for 10 min in Figs. 4.4(c) and 4.4(d).
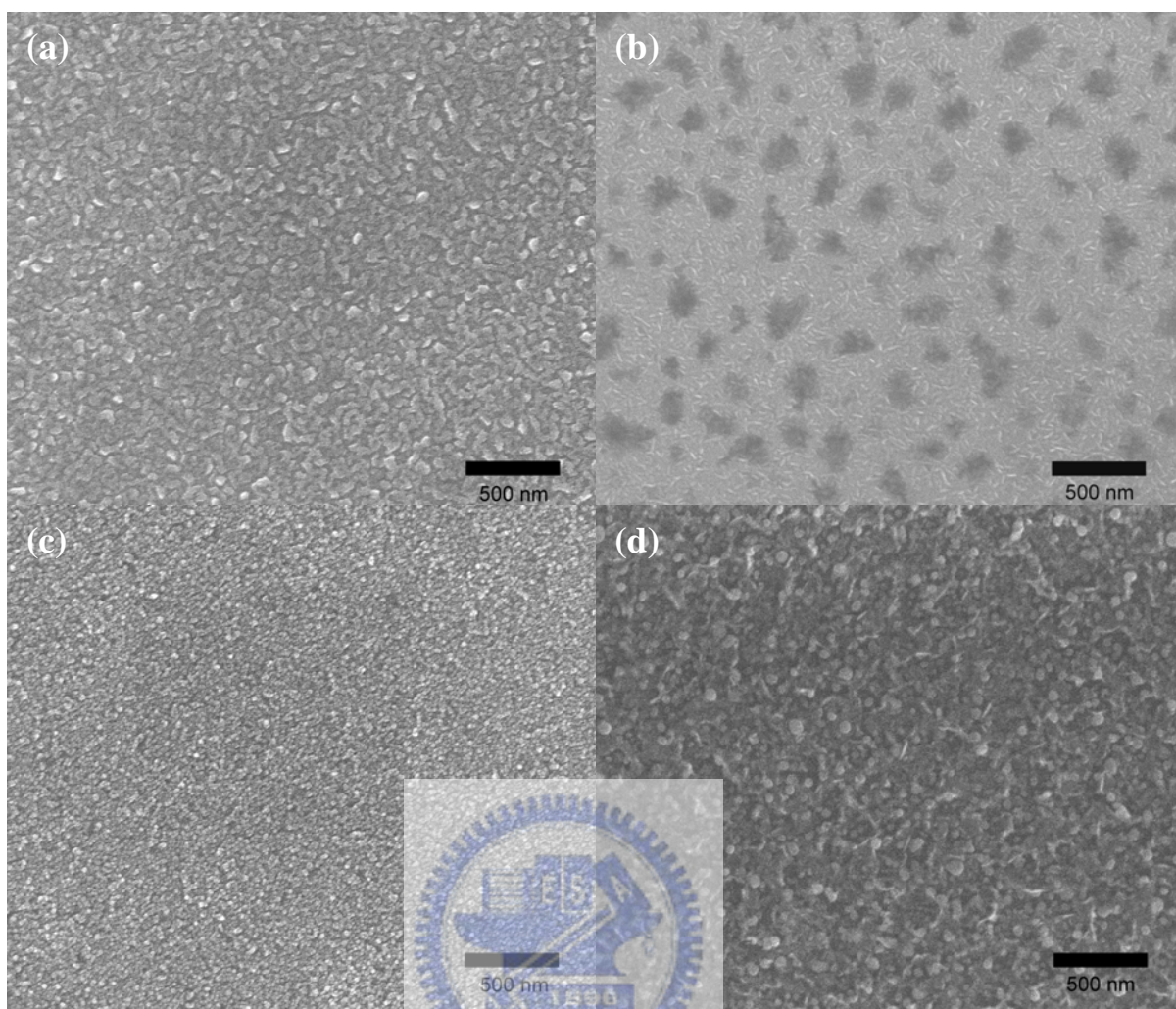
Fig. 4.4 Top-view SEM images of 10-nm-thick (a) oxidized (Ar:O$_2$ = 10:30) and (b) non-oxidized catalyst precursors with H-plasma pretreatment at 515°C for 8 min; and 10-nm-thick (c) oxidized and (d) non-oxidized catalyst precursor with H-plasma pretreatment at 591°C for 10 min. Other conditions: microwave power 600 W, working pressure 30 Torr and H$_2$ 100 sccm.

These figures indicate that the catalyst precursors coated under Ar + O$_2$ atmosphere give rise to a much smaller particle size after H-plasma pretreatment than that under pure Ar atmosphere. Effect of oxygen is basically to force formation of the loosely-packed metal oxides aggregates in the catalysts, where the aggregates may then be reduced under H-plasma to become smaller metal

particles. Higher oxygen content of 10 nm catalyst precursor was coated on the substrate under $Ar + O_2$ atmosphere ($Ar:O_2$ = 10:40 sccm/sccm) for smaller particles, but it shows no more effect.

4.1.3 XPS spectra

Figures 4.5(a) to (c) presents the results of the XPS of the H-plasma pretreated $CoCrPtO_x$ film formed by PVD, respectively, to study how catalyst precursor can form 2~3 nm nano-particles and prevent the agglomeration of catalysts as the buffer layer did in an earlier work [Delzeit-2001-368] [Zhong-2005-1558]. The spectra indicate that PtO_x, CrO_x and CoO_x phases are formed simultaneously in the as-deposited film during reactive sputtering deposition by PVD. Furthermore, the PtO_x associated with a peak at 74.05 eV ($4f_{7/2}$) comprises PtO (73.8 eV) and PtO_2 (74.6 eV), while CrO_x (577.4 eV) consists of CrO_2 (576.3 eV) and CrO_3 (578.3 eV), respectively. The spectrum presented in Fig. 4.5(a) shows that the Pt peak is shifted by 1 eV by pretreatment, indicating that most of the PtO_x atoms are reduced to Pt atoms in the H_2 atmosphere, but a small quantity of PtO_x remains. Most interestingly, the Cr phase in Cr_2O_3 remains, suggesting that the nano-particles from catalyst precursor results mostly from the reduction of PtO_x or CoO. However, the nano-sized catalysts are driven mainly by PtO_x as will be discussed in the following paragraph.
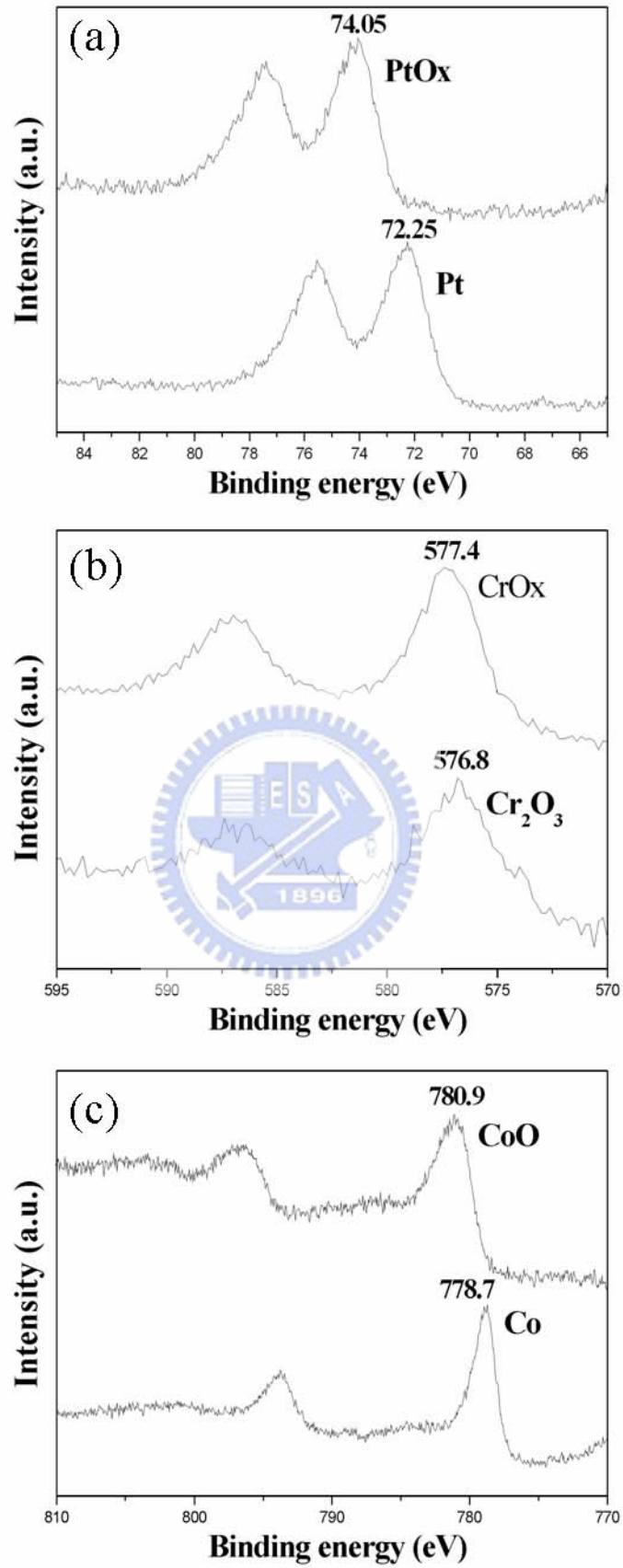
Fig. 4.5 XPS spectra of as-deposited CoCrPtO$_x$ film (upper curve) by PVD and after H-plasma pre-treated CoCrPtO$_x$ film (lower curve).

Recently, PtO_x has been demonstrated to be an active layer for use in the next generation of optical storage media applications [Kim-2003-1701], from which, oxygen is released after prolonged laser heating to compress the adjacent layers to form pits as recording marks, which consist of oxygen bubble gas and fine Pt nano-particles. Therefore, the exploding phenomenon associated with the reduction of PtO_x (PtO/PtO_2) may cause the formation of very fine particles and such self-assembly behavior may depend on the process temperature. In this experiment, a pre-treatment temperature that is too low (below 500 ^{o}C) results in an incomplete reduction of an oxidized CoCrPt film. In this case, non-uniform large catalytic particles are formed, and only MWNTs can be synthesized. The oxidized CoCrPt film has a higher critical self-assembly temperature than PtO_x (~500 ^{o}C), which difference is determined by the difference between the compositions.

With respect to the role of Cr, Cr_2O_3 can inhibit the agglomeration of particles [Shaijmon-2005-192]. Hence, it is believed to play a role in suppressing the agglomeration of catalytic particles in the self-assembly process. The Co element has an essential role in the dissolubility and precipitation of carbon species in the SWNTs growth because the dissolubility of carbon in Cr_2O_3 and Pt is rather small. The earlier work demonstrates that the pure Co catalytic nano-particles can also be formed by the reduction of CoO that is prepared as a

chemical complex solution. However, the large sizes distribution and low density of the particles do not support SWNTs growth. The self-assembly mechanism that involves the exploding effect associated with the reduction of $CoCrPtO_x$ film enables the size and distribution of the catalysts to be manipulated to fabricate as-grown SWCNT with the desired morphology by controlling the composition, thickness and H-plasma pre-treatment temperature of the film. The effect of the composition of CoCrPt on the self-assembly of nano-particles must be discussed in the future.

4.1.4 Morphology differences among various catalyst precursors

Additionally, to verify more carefully whether the effect is mainly resulted from PtO_2, the as-deposited 5-nm-think Co and $CoCrO_x$ film are prepared as comparison to perform the experiment under the same process condition. The results of H-plasma pretreated 5-nm-thick Co, $CoCrO_x$ and $CoCrPtO_x$ films are illustrated in Figs. 4.6(a), (b) and (c), and show the particle size order is Co, $CoCrO_x$ and $CoCrPtO_x$. From comparing particle size of Co and $CoCrO_x$, we confirm that Cr_2O_3 has effective capability to inhibit nano-particles agglomeration. Moreover, comparison of $CoCrO_x$ and $CoCrPtO_x$ reveals the reduction of PtO_x (PtO/PtO_2) may cause the formation of very fine particles. Although $CoCrO_x$ can obtain smaller particles than Co, it is not a good candidate
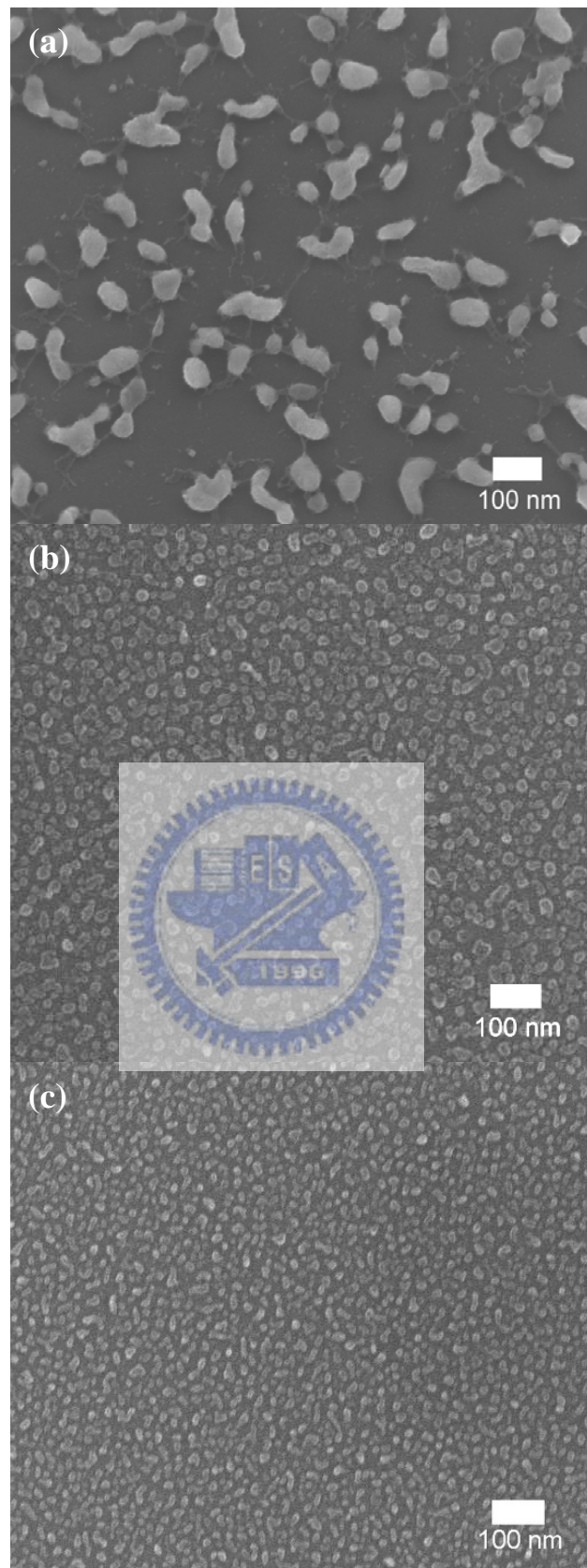
Fig. 4.6 Top view SEM images of after H-plasma pretreated 5-nm-thick (a) Co, (b) $CoCrO_x$ and (c) $CoCrPtO_x$ films.

as catalyst to synthesize SWNTs. Because there are no SWNTs can be observed

in our experiments.

4.2 Morphologies and Raman spectra of the carbon nanostructures

4.2.1 Morphologies and Raman spectra of carbon nanostructures

Figures 4.7(a) to 4.7(f) illustrate typical FESEM morphologies of the

as-grown SWNTs on silicon wafer with different catalyst precursor thickness: (a)

10 nm, (b) 5 nm (c) 3 nm, (d) 2 nm, (e) 1 nm and (f) 1 nm with buffer layer. To

confirm the types of CNTs precisely, Fig. 4.8 shows the Raman spectrum of

as-grown SWNTs film, respectively. The RBM peaks in the Raman spectrum

[Fig. 4.7] indicate the presence of SWNTs in Figs. 4.7(d), (e) and (f). Therefore,

we demonstrate that vertically aligned SWNTs are successfully synthesized

using $CoCrPtO_x$ catalyst precursor with 2 nm and 1 nm thickness. And very high

I_G/I_D ratio (43/1) is obtained by 1-nm-thick catalyst precursor with 10-nm-thick

AlON buffer layer.

Figures 4.9(a) and 4.9(b) show the TEM images of as-grown SWNTs with

1-nm-thick $CoCrPtO_x$ film and 10-nm-thich AlON buffer layer. The results

indicate that the nanotubes are grown as SWNTs bundles with diameters of 2 to

3 nm, which resembles the diameter of catalyst particles observed by HRTEM.

Therefore, each SWCNT maybe grown from individual catalytic nano-particles

and the diameter of tubes is determined by sizes of the catalysts. Hardly any
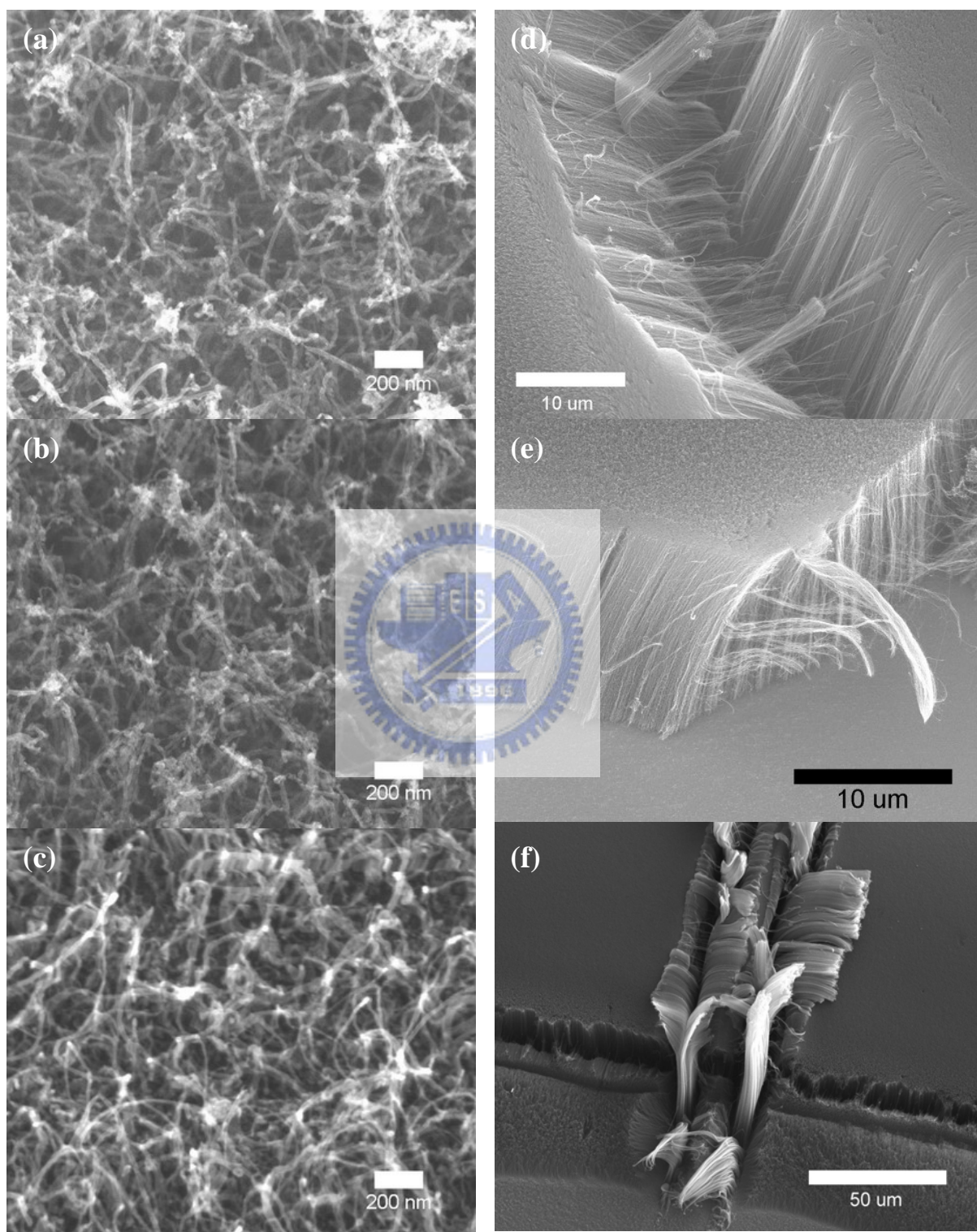
Fig. 4.7 SEM images of the as-grown SWNTs on silicon wafer with different catalyst precursor thickness: (a) 10 nm, (b) 5 nm (c) 3 nm, (d) 2 nm, (e) 1 nm and (f) 1 nm with buffer layer.
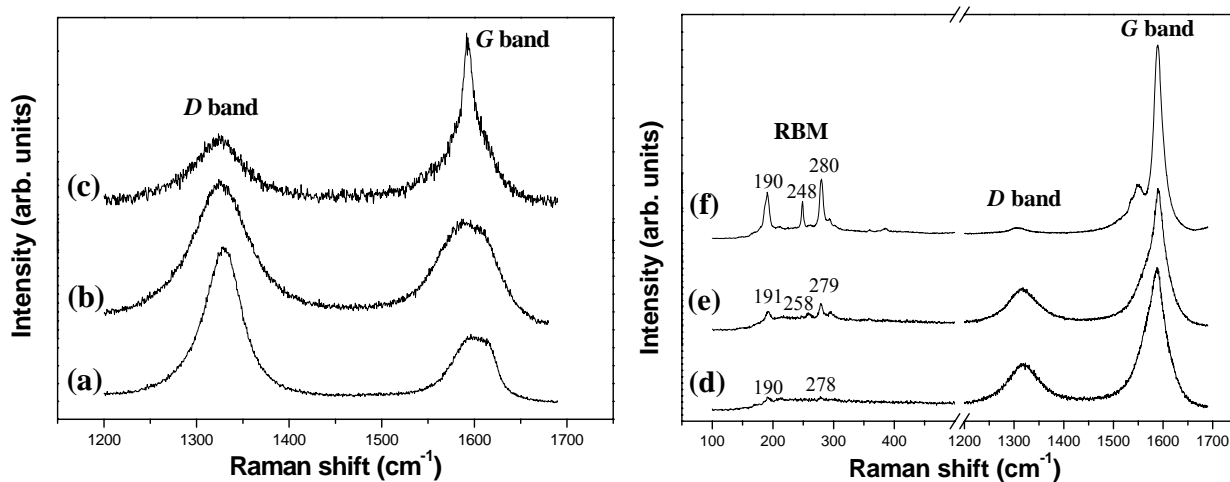
Fig. 4.8 Raman spectra of the as-grown SWNTs film on silicon wafer with different catalyst precursor thickness: (a) 10 nm, (b) 5 nm (c) 3 nm, (d) 2 nm and (e) 1 nm. The RBM peaks and very high intensity ratio of G-band / D-band (43:1) are found in the (f) 1-nm-thick catalyst precursor with buffer layer.
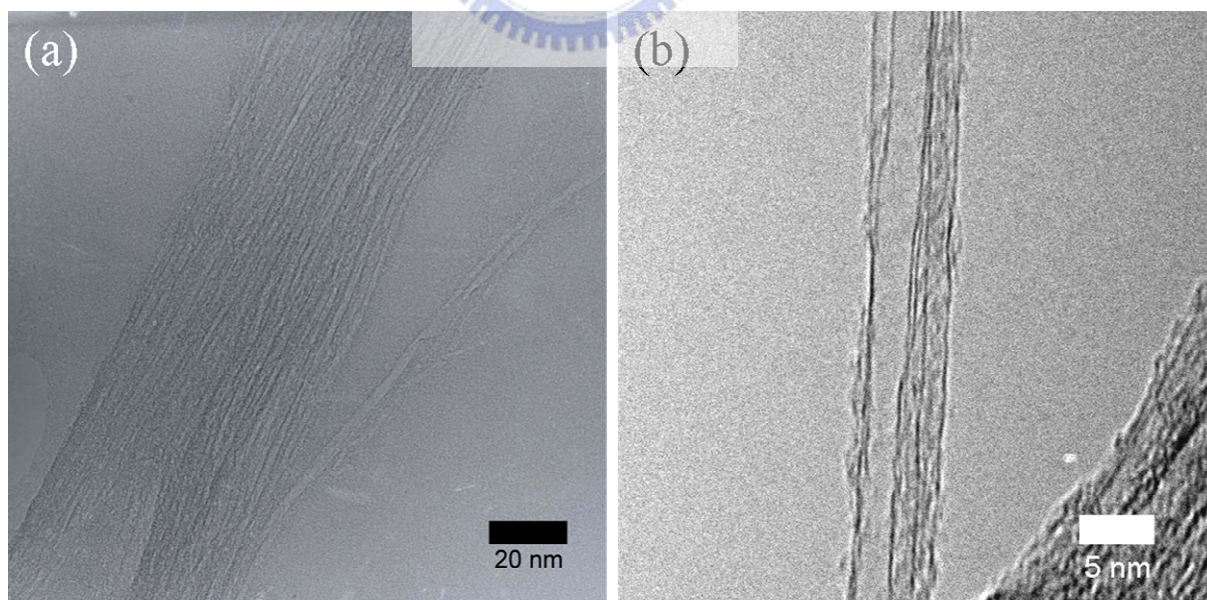
Fig. 4.9 HRTEM images of the typical as-grown SWNTs where the tubes are mainly bundle type and their diameters are ranged from 2~3 nm.

MWNT are founded by TEM and a very high I_G/I_D ratio (43/1) is obtained by Raman spectrum, which indicate the purification and high quality of SWNTs is good as obtained by arc-discharge which is high temperature precess.

The tilt-view of specimen presented in Figs. 4.10(a) and 4.10(b) display SWNTs film with an ultra-high density and a tube density that considerably exceeds that reported elsewhere [Zhong-2005-1558]. Figure 4.10(c) magnifies a portion of Fig. 4.10(b), to show the fabrication of bundles of aligned SWNTs. Figure 4.10(d) shows that vertically aligned SWNTs with a height of ~40 micrometer were successfully synthesized. Notably, the SWNTs film can be easily removed from substrate and the SWNTs film is very flexible and soft, likely the woolen blanket, as shown in Fig. 4.10(e). Figure 4.10(f) shows a fragment of Si substrate with catalyst precursor which well-aligned SWNTs are magically grown exhibits the powerful growth ability of $CoCrPtO_x$ catalyst precursor.

Vertically well-aligned SWNTs films with heights of ~50 micrometer are thus concluded to fabricate successfully under the condition. By contrast, entangled SWNTs rather than aligned tubes were found in the specimens that comprised a thicker as-deposited catalyst precursor film of over ~10 nm and MWNTs are easily observed by TEM. These results are consistent with that the catalyst precursor thickness must be control at ultra thin to enable SWNTs to be synthesized.
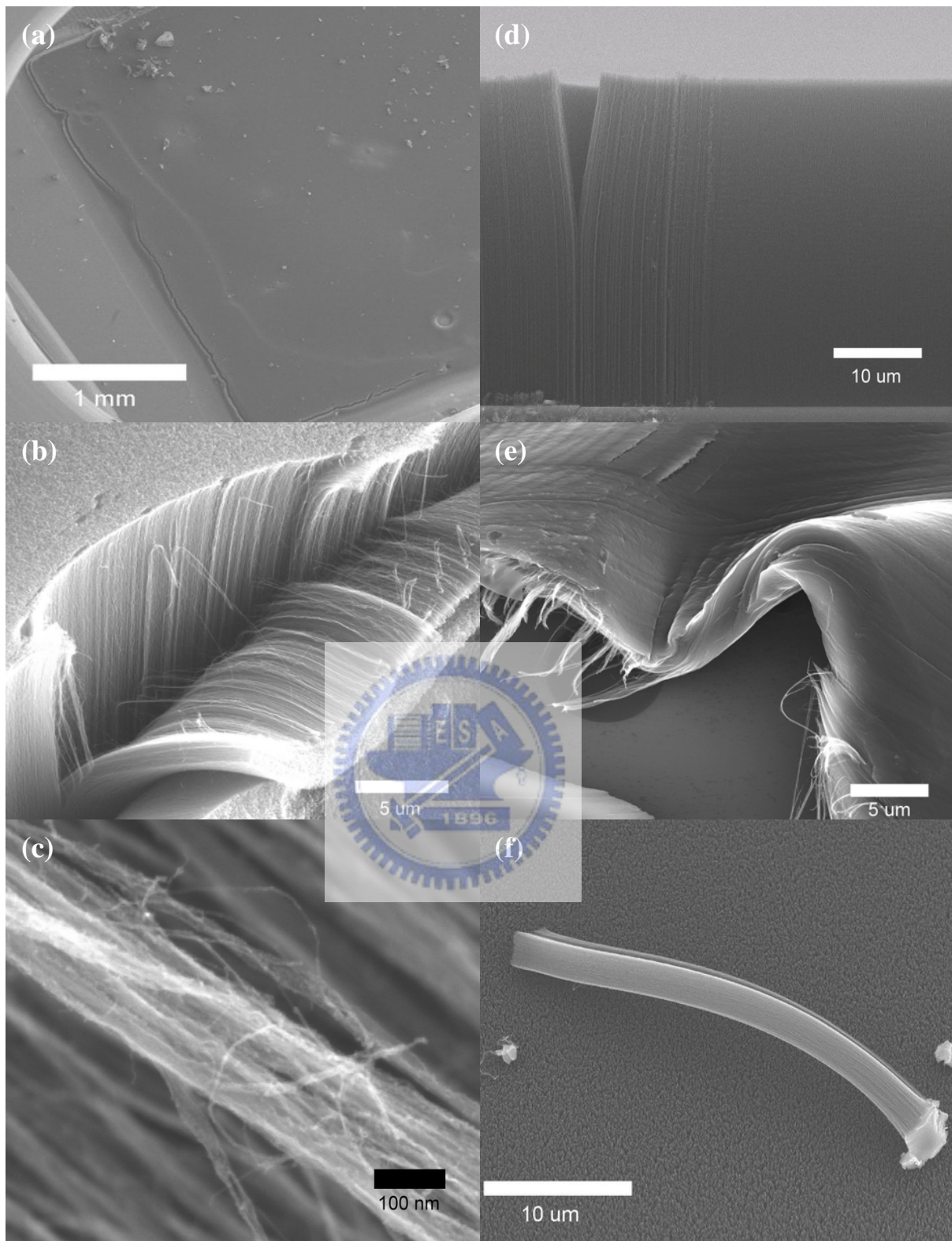
Fig. 4.10 Typical SEM micrographs of extremely dense and vertically aligned SWNTs film on silicon wafers: (a), (b) tilt-view, (c) is the high magnification image of (b), (d) cross-sectional view, (e) shows very flexible morphology and (f) a fragment of Si substrate, respectively.

4.2.2 Effect of specimen stacking sequences on carbon nanostructures

The schematic diagram of specimen placement in MPCVD is shown in Fig 3.4, and different placement gets different result. Sample A obtains the highest I_G/I_D ratio of as-grown SWNTs, because of the relative higher temperature by directly plasma bombardment to backside. But in sample C, only short and entangled SWNTs can be observed, as shown in Fig. 4.11. This is probably caused by plasma etching to SWNTs during growth process. Sample D gets the highest SWNTs because of the rough backside surface of Si wafer which gives more space for SWNTs growth. Although the placement of specimen will affect the result of SWNTs growth, the degree is relative slight comparing with other conditions, such as catalyst precursor, gas ratio, etc.
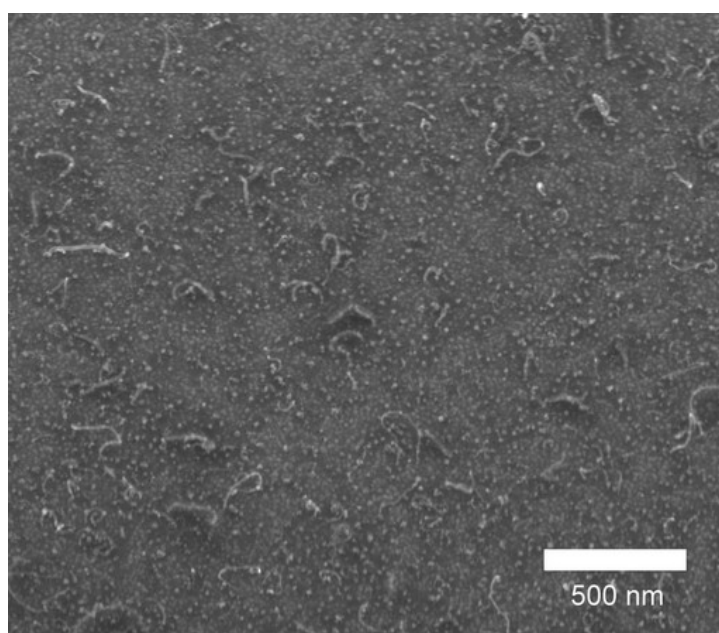
Fig. 4.11 Top-view SEM image of short and entangled SWNTs of sample C.

4.2.3 Morphologies of the two-step grown carbon nanostructures

Two-step growth of SWNTs using 1st-grown SWNTs removed substrate is attempted under the same H-plasma pretreatment and growth conditions of section 4.2.1. Figure 4.12 show the SEM image and Raman spectrum of two-step grown carbon nanostructure, and the results shows that well-aligned SWNTs are successfully grown again and indicate the base growth mechanism. From the low magnification SEM top view, it is observed that vertical well-aligned SWNTs are successfully synthesized again, but randomly oriented cracks appear on all two-step SWNT samples, as shown in Fig. 4.12(a). In contrast, cracks were never observed on previous samples. The most probably reason for these cracks is the insufficient density of two-step SWNTs by poisonous catalyst which amorphous carbon atoms are not completely removed in 10 minutes H-plasma pretreatment time. Therefore, the Van der Waals attraction among SWNTs creates cracks by contraction when the samples are cooled from 600°C to room temperature. Hence, we extend the H-plasma pretreatment time to 15 minutes to eliminate the amorphous carbon atoms on the catalysts, and then vertical well-aligned SWNTs without cracks are synthesized. The Raman spectrum of two-step SWNTs with 15 minutes H-plasma pretreatment time is shown in Fig. 4.12(b). It is of interest that the RBM peak becomes singular centralization at Raman shift of 281 cm^{-1}, indicates that the

diameter of two-step SWNTs are highly uniform. This is probably resulted from

the uniform catalyst particle size by longer H-plasma pretreatment time. Thus,

extremely dense and vertical well-aligned SWNTs (40~50 μm) are successfully

re-grown and the average yield rate one cycle is ~0.2 mg/cm^2.
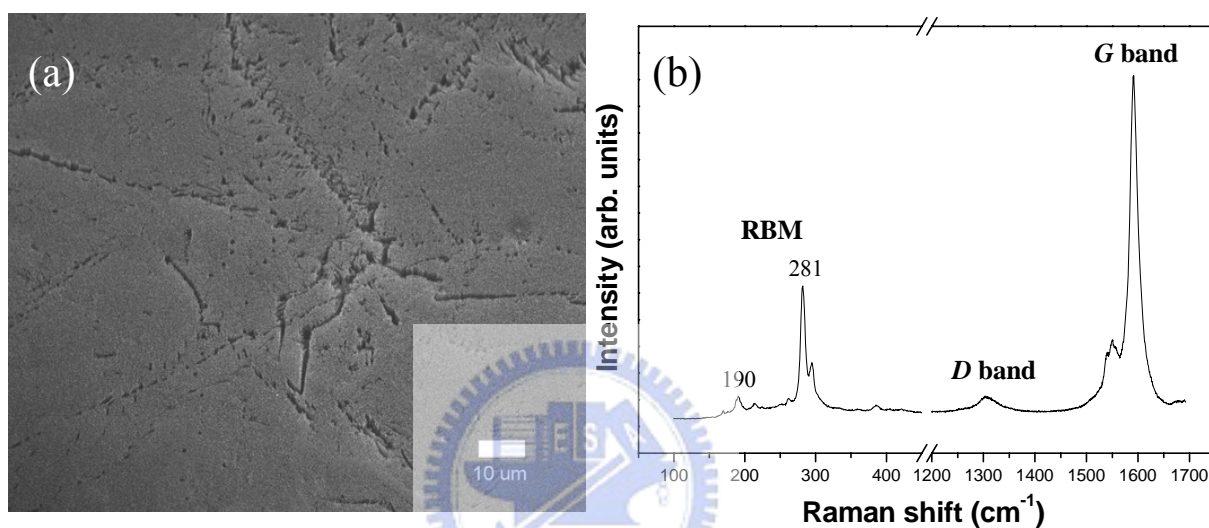
Fig. 4.12 (a) Top-view SEM image of re-grown SWNTs with insufficient
pretreatment time. (b) Raman spectrum of re-grown SWNTs with suitable
pretreatment time.

4.3 Effect of scanning local laser heating pretreatment on CNTs growth

4.3.1 Morphologies of the laser-pretreated catalyst precursors

Figure 4.13(a) shows the morphology of the 1-nm-thick catalyst precursor

deposited PC substrate after local laser heating pretreatment. The laser heating

region which rises above other area is about 1-μm-diameter size. Figure 4.13(b)

is high magnification image of Fig. 4.13(a), shows there are many tiny seams on

the catalyst surface, which is probably result from the exploding reduction of PtO$_2$. The morphology of laser heating region after 10 minutes 350 °C H-plasma pretreatment is shown in Fig. 4.13(c). It is apparent that the catalyst precursor at pattern region becomes well-distributed nano-particles and other area only exist a small amount disorder and bigger particles. We firmly believe that these tiny seams increase the plasma etching area and many defects occur on their surface during the process of PtO$_2$ exploding reduction which enhances the etching ability of H-plasma. Thus, the catalyst nano-particles are successfully synthesized at 350 °C by laser heating and then H-plasma pretreatment. AlON buffer layer was not employed here, because it was thoroughly damaged after local laser heating pretreatment.
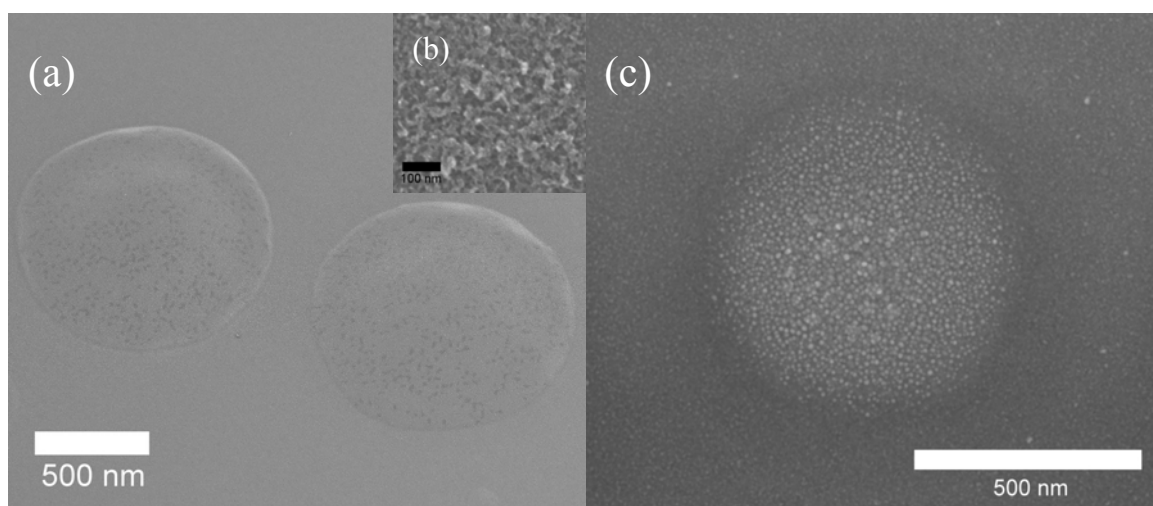
Fig. 4.13 Top-view SEM images of catalyst precursor (a), (b) after laser ablation pretreatment and (c) after 10 min. 350 °C H-plasma pretreatment.

4.3.2 Morphologies and Raman spectra of carbon nanostructures

Top-view SEM image and Raman spectrum of low temperature grown SWNTs at 373 °C are shown in Figs. 4.14(a) and (b). From these, we confirm that SWNTs are successfully synthesized at laser heating region. Although many outcomes must be improved like the entangled SWNTs, weak RBM peak and low I_G/I_D ratio, etc, the feasibility for selective growth of well-aligned SWNTs and for compatibility with IC processes at low temperature is expectable in the future. The lowest temperature to synthesize SWNTs is 373 °C and MWNTs is 262 °C. And these are never reached in the past research in the world.
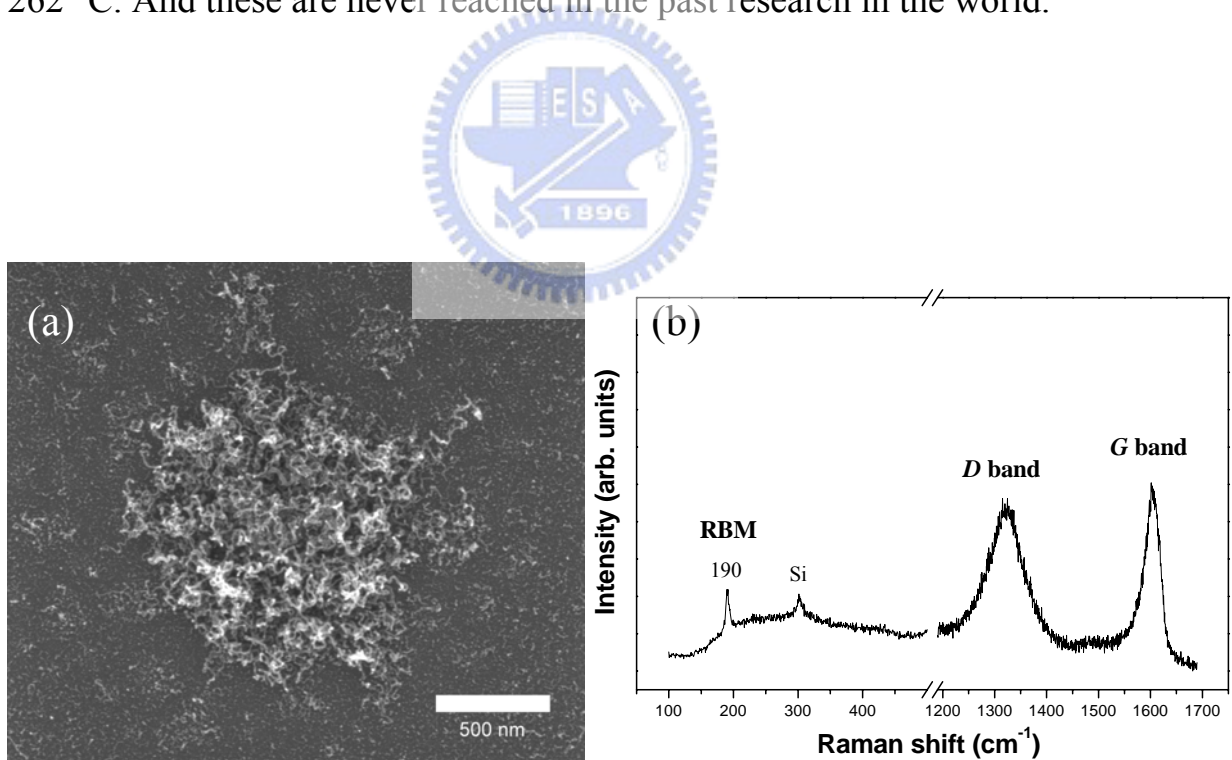
Fig. 4.14 (a) Top-view SEM image and (b) Raman spectrum of low temperature grown SWNTs at 373 °C

4.4 Growth mechanisms of SWNTs

4.4.1 High temperature growth mechanism

The EDX analysis is used to study the growth mechanism of as-grown vertically well-aligned SWNTs by novel $CoCrPtO_x$ catalyst precursor, and the result [Fig. 4.15] shows the catalysts existed in the SWNTs removed substrate, indicates the growth mechanism of as-SWNTs is base-growth mechanism. This is confirmed by the interestingly two-step growth method which 1st-grown SWNTs is removed from substrate to grow SWNTs again under longer H-plasma pretreatment and the same growth conditions. The surface and body diffusion were both expected in the high temperature growth mechanism [Hofmann-2005-036101].

The TEM results indicate that each SWNT is grown from individual catalyst nano-particle and tube diameter is determined by catalyst size. With respect to the fabrication of the extremely dense SWCNT film, highly dense very fine catalytic particles is proposed to be formed uniformly by H-plasma pre-treatment and aligned tubes are then grown vertically, constrained among the tubes. By contrast, if the distribution densities of fine catalytic particles are low, entangled SWCNT are formed.

4.4.2 Low temperature growth mechanism

Hofmann et al. proposed the surface diffusion: The low activation energy path for nanotube growth [Hofmann-2005-036101], find low activation energy of 0.4 eV for carbon surface diffusion on Ni and Co (111) planes, much lower than for bulk diffusion. In MPCVD, the plasma ionizes the gas and creates new and more reactive species, such as radicals, in the gas phase and/or the catalyst surface, as well as to cause a local surface heating that enables an efficient adsorption and diffusion of carbon atoms at low substrate temperatures. The plasma atmosphere may influence the detailed catalyst surface kinetics in many ways and may also supply carbon from the gas phase for SWNTs growth. This allows a reduction of the growth activation energy, as, e.g., atomic carbon can chemisorb directly on the catalyst. Therefore, we suggest that diffusion of carbon on the catalyst surface is the rate determining step at low temperatures. The effect of the plasma is to increase the dissociation of CH_4, and etch any a-C, which may deposit on top of the catalyst particle, thereby providing a steady supply of carbon atoms at the top surface of the catalyst particle. At low temperatures, the solubility of C in Co is low, so the amount of carbon diffusing through the particle is very limited. However, carbon atoms adsorbed at the top surface of the catalyst particle can diffuse along the surface, where their motion is much faster. Carbon then segregates at the bottom of the particle, forming graphitic planes. This process allows SWNTs to grow at such low temperatures.
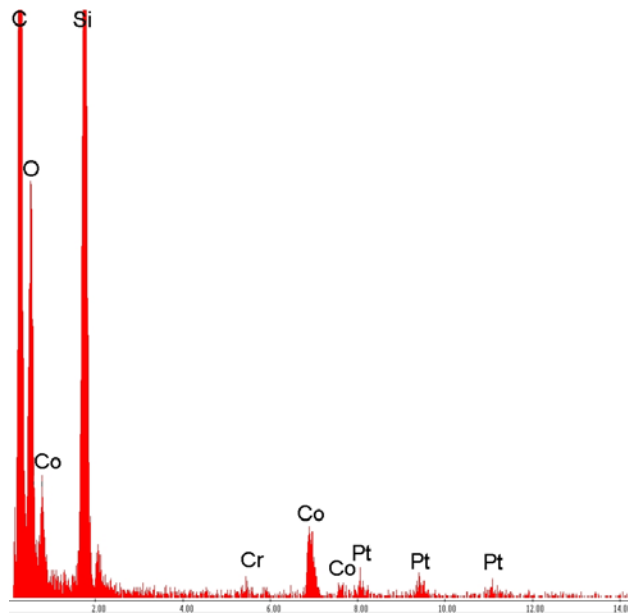
Fig. 4.15 EDX analysis of as-grown SWNTs removed substrate.

4.5 Properties analyses of SWNTs

4.5.1 Field emission properties

The field emission current density as a function of electric field for the as-grown well-aligned SWNT of sample A5 (CoCrPtO$_x$ 1 nm) is shown in Fig. 4.16. It shows a turn on voltage of 4.6 V/μm (0.01 mA/cm^2) and the current density of 6 mA/cm^2 (7.2 V/μm). In our experiments, the tube packing density is obviously higher and results in lower intertube distances. In order to avoid the field screening effect, a lower packing density of CNTs is favorable.
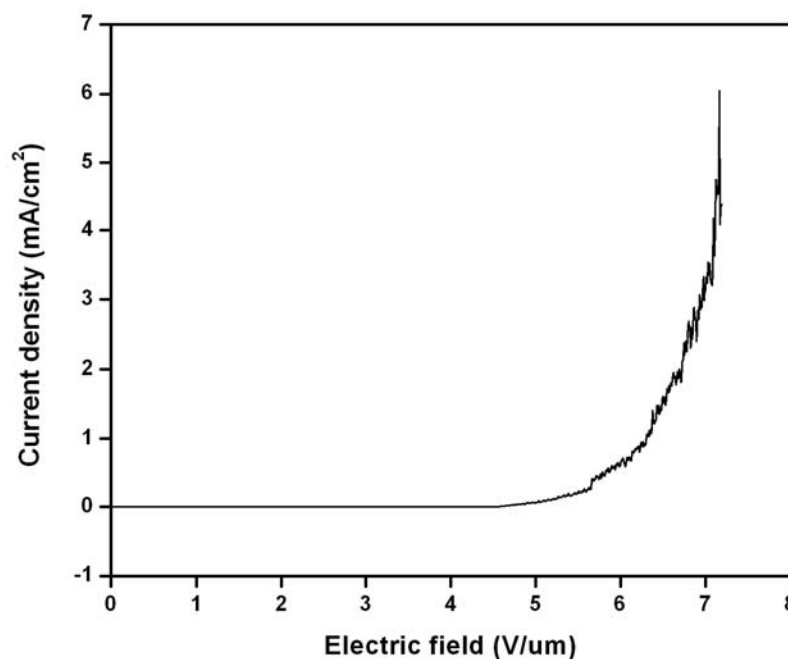
Fig. 4.16 Field emission current density as a function of electric field for the SWNTs

4.5.2 Oxidation resistance

Thermo-gravimetric analysis (TGA) is implemented on 5 mg of the as-grown SWNTs (ramp rate, 10°C/min in air, 30 sccm/min), as shown in Fig. 4.17. The combustion range of the SWNTs was 586°C to 691°C, with the peak weight reduction occurring at 650°C, a result very similar to that of purified, high-quality SWNTs synthesized by a laser-oven method. We believe that the small initial weight increase is due to physisorption, supported by the fact that the weight returns to its initial value by subsequent annealing. No measurable residue remained after heating above 700°C, indicating very high purity.
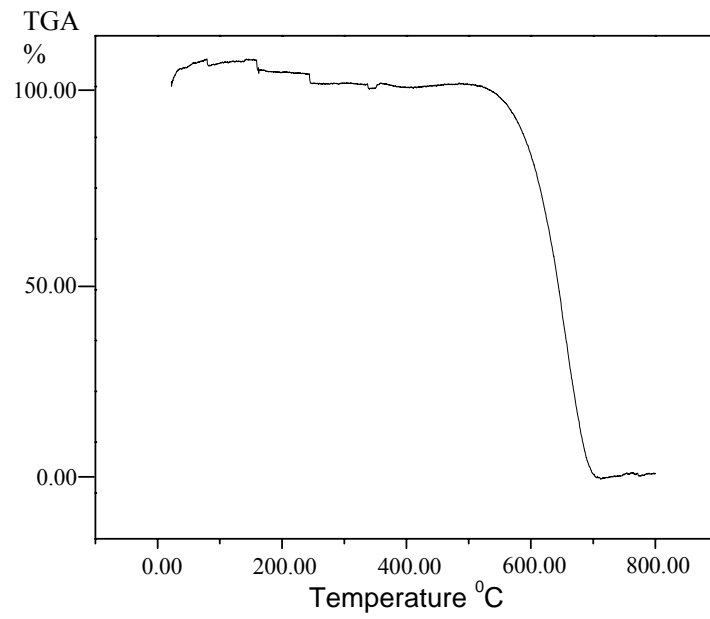
Fig. 4.17 Thermo-gravimetric properties of as-grown SWNTs. (5 mg, ramp rate, 10°C/min)

Chapter V
Conclusions

In this work, the $CoCrPtO_x$ film was successfully used as catalyst precursor to grow the well-aligned SWNTs with high tube number density by MPCVD. The main mechanism to form SWNTs is due to the fact that the PtO_x in the $CoCrPtO_x$ precursor can be decomposed during pretreatment to promote miniaturization of the Co-catalyst particle due to explosive effect of the reaction. Moreover, Cr_2O_3 in the precursor can act to separate the Co-catalyst nanoparticles from agglomeration. The process also takes the advantage of recycling the catalyst-coated substrate to minimize the processing cost.

These SWNTs exhibit competitive field emission properties, i.e. turn on voltage of 4.6 V/µm (at 0.01 mA/cm^2) and the current density of 6 mA/cm^2 (at 7.2 V/µm). Raman spectra indicate that the I_G/I_D ratio of these SWNTs can be reached to $\sim$ 43, indicating a good quality. The results of TGA analysis in air show that these SWNTs can resist oxidation up to $586^{\circ}C \sim 691^{\circ}C$, which are much higher than the reported temperatures ($\sim 350^{\circ}C$) in the literature, and are comparable with that for the purified SWNTs synthesized by a laser-oven method.

The scanning local laser heating pretreatment was successfully used to

decrease the CNTs deposition temperature to 373°C, which is based on heating the local area to a higher temperature to form nanoparticles and maintaining the substrate at lower temperature.

Chapter VI
Future prospects

1. The effect of catalyst composition on SWNTs growth.

2. Feasibility study of SWNTs growth with higher length at large area.

3. Synthesize SWNTs on plastic substrate.

References

B

1. Bachtold, A., P. Hadley, T. Nakanishi, and C. Dekker, Science, 294, (2001), 1317-1320, "Logic Circuits with Carbon Nanotube Transistors".

2. Berber, Savas, Young-Kyun Kwon,* and David Tománek, PHYSICAL REVIEW LETTERS, 84, (2000), 4613-4616, "Unusually High Thermal Conductivity of Carbon Nanotubes".

3. Bethune, D. S., Kiang C. H., Vries M. S. de, Gorman G., R. Savoy, J. Vazquez, and R. Beyes, Nature, 363, (1993), 605-607, "Cobalt- Catalysed growth of carbon nanotubes with single-atomic-layer wall".

4. Baker, R. T. K. and P. S. Harris, in Chemistry and Physics of Carbon, edited by P. L. Walker and P. A. Thrower ~Marcel Dekker, New York, (1978), Vol. 14.

5. Birkett, P.R., A. J. Cheetham, B. R. Eggen, J. P. Hare, H. W. Kroto, Chemical Physics Letter, 281, (1997), 111-114,"Transition metal surface decorated fullerenes as possible catalytic agents for the creation of single walled nanotubes of uniform diameter".

C

1. Collins, P. G., M. S. Arnold, and P. Avouris, Science, 292, (2001), 706-709, "Engineering Carbon Nanotubes and Nanotube Circuits Using Electrical

Breakdown".

2. Che, Jianwei, Tahir Cagın and William, Nanotechnology, 11, (2000), 65–69, "A Goddard III Thermal conductivity of carbon nanotubes".

3. Choi, W. B., Chung D. S., Kang J. H., Kim H. Y., Jin Y. W., Ha I. T., Y. H. Lee, Jung J. E., Lee N. S., Park G. S., and Kim J. M., Appl. Phys. Lett., 75, (1999), 3129-3131, "Fully sealed, high-brightness carbon-nanotube field-emission display".

D

1. Delzeit, L., B. Chen, A. Cassell, R. Stevens, C. Nguyen, and M. Meyyappan, Chem. Phys. Lett. 348, (2001), 368-374, Multilayered metal catalysts for controlling the density of single-walled carbon nanotube growth".

2. Dresselhaus, M. S., G. Dresselhaus, P. C. Eklund, "Science of Fullerences and Carbon Nanotubes" (Academic Press, New York, 1996), P756.

3. Dai, H., A. G. Rinzler, P. Nikolaev, A. thess, D. T. Colber, and R. E. Smalle, Chem. Phys. Lett., 260, (1996), 471-475, "Single-walled nanotubes produced by metal catalyzed disproportionation of carbon monoxide".

4. Dresselhaus, M. S., G. Dresselhaus, A. Jorio, A.G. Souza Filho, R. Saito, R. saito, carbon, 35, (2002), 2043–2061, "Raman spectroscopy on isolated single wall carbon nanotubes".

5. Derycke, V., Martel R., Appenzeller J., and Ph. Avouris, Nano Letter, 1,

(2001), 453-456, "Carbon Nanotube Inter- and Intramolecular Logic Gates".

6. Dai, H., Hafner J. H., Rinzler A. G., Colber D. T., and Smalley R. E., Nature, 384, (1996), 147-150, "Nanotubes as nanoprobes in scanning probe microscopy".

_E_

1. Eric W. Wong, Paul E. Sheehan, Charles M. Lieber, Science, 277, (1997), 1971-1975, "Nanobeam mechanics: Elasticity, strength, and toughness of nanorods and nanotubes".

_G_

1. Groning O., O. M. Kuttel, Ch. Emmenegger, P. Groning, and L. Schlapbach, J. Vac. Sci. Technol. B, 18, (2000), 665-678, "Field emission properties of carbon nanotubes".

2. Guo, T., P. Nikolaev, A. Thess, D. T. Colbert, and R. E. Smalley, Chem. Phys. Lett., 243, (1995), 49-54, "Catalytic Growth of Single-walled Nanotubes by Laser Vaporization".

3. Gavillet, J., A. Loiseau, C. Journet, F. Willaime, F. Ducastelle, and J.-C.Charlier, Physical Review Letters, 87, (2001), 275504-1 -275504-4, "Root-Growth Mechanism for Single-Wall Carbon Nanotubes".

4. Gorbunov, A., O. Jost , W. Pompe , A. Graff, Carbon, 40, (2002)

113–118, "Solid–liquid–solid growth mechanism of single-wall carbon Nanotubes".

5. Gao, B., A. Kieinhammes, X. P. Tang, C. Bower, L. Fleming, Y. Wu and O. Zhou, Chem. Phys. Lett., 307, (1999), 153-157, "Electrochemical intercalation of single walled carbon nanotubes with lithium"

H

1. Hamada Noriaki, Shin-ichi Sawada, and Atsushi Oshiyama, Phy. Rev. Letters, 68, (1992), 1579-1581, "New One-diamensional Conductors: Graphitic Microtubules".

2. Hofmann, S., G. Csanyi, A. C. Ferrari, M. C. Payne and J. Robertson, PHYSICAL REVIEW LETTERS, 95, (2005), 036101, "Surface Diffusion: The Low Activation Energy Path for Nanotube Growth"

I

1. Iijima, S., Nature, 354, (1991), 56-58, "Helical microtubules of graphitic carbon"

K

1. Kroto H.W., J.R. Heath, S.C. O'Brien, R.F. Curl & R.E. Smalley, Nature, 318, (1985), 162-163, "C_{60}:Buckminsterfullerence"

2. Kim J., I. Hwang, D. Yoon, I. Park, D. Shin, T. Kikukawa, T. Shima, and J. Tominaga, Appl. Phys. Lett., 83, (2003), 1701-1703, "Super- resolution by

elliptical bubble formation with PtOx and AgInSbTe layers".

3. Kurt, R., J. M. Bonard, A. Karimi, Carbon, 39, (2001), 1723-1730, "Morphology and field emission properties of nano-structured nitrogenated carbon films produced by plasma enhanced hot filament CVD".

4. Kuo, C. T., T. K. Chao, "Nano-structured materials science" (Chwa technology books), (2004), P.9-10~P.9-14.

5. Kong J., A. M. Cassell, and H. Dai, Chem. Phys. Lett., 292, (1998), 567-574, "Chemical vapor deposition of methane for single-walled carbon nanotubes".

1. Kuo, Cheng Tzu, Chao Hsun Lin and An Ya Lo, Dia. Rel. Mat., 12, (2003), 799-805, "Feasibility studies of magnetic particle embedded carbon nanotubes for perpendicular recording media".

2. Lee, C. J., S. C. Lyu, Y. R. Cho, J. H. Lee, and K. I. Cho, Chem. Phys. Lett., 341, (2001), 245-249, "Diameter-controlled growth of carbon nanotubes using thermal chemical vapor deposition".

3. Lin, C. H., H. L. Chang and C. T. Kuo, Dia. Rel. Mater., 11, (2002), 922-926, "Growth meachanism and properties of the large area well-aligned carbon nanostructures deposited by microwave plasma ECRCVD".

4. Liu, C., Y. Y. Fan, M. Lu, H. T. Cong, H. M. Cheng, M. S. Dresselhaus,

Science, 286, (1999), 1127-1129, "Hydrogen Storage in Single-Walled Carbon Nanotubes at Room Temperature".

Q

1. Odom Teri Wang, Jin-Lin Huang, Philip Kim and Charles M. Lieber, Nature, 391, (1998), 62-64, "Atomic structure and electronic properties of single-walled carbon nanotubes".

P

1. Pan Z. W., S. S. Xie, L. Lu, B. H. Chang, L. F. Sun, W. Y. Zhou, G. Wang, and D. L. Zhang, Appl. Phys. Lett., 74, (1999), 3152-3154, "Tensile tests of ropes of very long aligned multiwall carbon nanotubes".

Q

1. Qin, L. C., D. Zhou, A. R. Krauss, and D. M. Gruen, App. Phys. Lett., 72, (1998), 3437-3439, "Growing carbon nanotubes by microwave plasma-enhanced chemical vapor deposition".

R

1. Rao, A. M., E. Richter, Shunji Bandow, Bruce Chase,P. C. Eklund, K. A. Williams, S. Fang, K. R. Subbaswamy,M. Menon, A. Thess, R. E. Smalley, G. Dresselhaus,andM. S. Dresselhaus, science, 275, (1997), 187-191, "Diameter-Selective Raman Scattering from Vibrational Modes in Carbon Nanotubes".

2. Raravikar, Nachiket R., Pawel Keblinski, Apparao M. Rao, Mildred S. Dresselhaus, Linda S. Schadler and Pulickel M. Ajayan, PHYSICAL REVIEW B, 66, (2002), 235424-1~235424-9, "Temperature dependence of radial breathing mode Raman frequency of single-walled carbon nanotubes".

$\underline{S}$

1. Shaijumon M. M., N. Bejoy, and S. Ramaprabhu, Appl. Sur. Sci., 242, 192, (2002), 192-198, "Temperature dependence of radial breathing mode Raman frequency of single-walled carbon nanotubes".

2. Saito R., Fujita M., Dresselhaus G., and Dresselhaus M. S, Appl. Phys. Lett., 60, (1992), 2204-2206, "Electronic structure of chiral graphene tubules".

3. Spindt, C. A., I. Bride, L. Humprey and E. R. Westerberg, „J. Appl. Phys., 47, (1976), 5248, " Physical properties of thin-film field emission cathodes molybdenum cones"

4. Satio, Y, Carbon, 33, (1995), 979-988, "Nanoparticles and filled nanocapsules".

5. Saito, Yahachi, Mitsumasa Okuda, Naoya Fujimoto Tadanobu Yoshikawa, Masato Tomita, and Takavoshi Hayashi, Jpn. J. Appl. Phys, 33, (1994), L526-L529, "Single-wall carbon nanotubes growing radially from Ni fine particles formed by arc evaporation".

6. Saito, Y., S. Uemura, and K. Hamaguchi, Jpn. J. Appl. Phys., 37, (1998),

L346-348, "Cathode Ray Tube Lighting Elements with Carbon Nanotube Field Emitters".

7. Sander, J. Tans, A. R. M. Verschueren, and C. Dekker, Nature, 393, (1998), 49-52, "Room-temperature transistor based on a single carbon nanotube".

T

1. Tsai, M. H., M.S. Thesis, (2001), Mat. Res. Lab., MSE, NCTU, "Deposition mechanisms and properties of large area well-aligned carbon nanotubes by catalyst-assisted ECR-CVD method".

2. Thess, Andreas, Lee, Roland, Nikolaev, Pavel, Dai, Hongjie, Science, 273, (1996), 483-487, "Crystalline ropes of metallic carbon nanotubes".

3. Tuinstra, F., and J. L. Koenig, The journal of chemical, 53, (1970), 1126-1130, "Raman Spectrum of Graphite".

W

1. Wildoer, Jeroen W. G., Liesbeth C. Venema, Andrew G. Rinzler†, Richard E. Smalley and Cees Dekker, 391, (1998), 59-62, "Electronic structure of atomically resolved carbon nanotubes".

2. Wong, S. S., E. Joselevich, A. T. Woolley, C. L. Cheung, C. M. Lieber, Nature, 394, (1998), 52-55, "Covalently functionalized nanotubes as nanometre-sized probes in chemistry and biology".

3. W.H. Wang, Y.R. Peng, C.T. Kuo, Diamond & Related Materials, (2006), "Low temperature growth mechanism of SWNTs networks by buffer layer assisted MPCVD".

4. W.H. Wang, Y.R. Peng, C.T. Kuo, Diamond & Related Materials, 14, (2005), 1906-1910, "Effects of buffer layer materials and process conditions on growth mechanisms of forming networks of SWNTs by microwave plasma chemical vapor deposition".

_Y_

1. Yu, M, O. Lourie, M. Dyer, K. Mooni, T. Kelly, R. S. Ruoff, Science, 287, (2000), 637-640, **"St**rength and Breaking Mechanism of Multiwalled Carbon Nanotubes Under Tensile Load".

2. Yun Sung Woo, Duk Young Jeon, In Taek Han, Young Jun Park, Ha Jin Kim, Jae Eun Jung, Jong Min Kim, Nae Sung Lee, J. of Appl. Phy., 94, (2003), 6789-6795, "Structural characteristics of carbon nanorods and nanotubes grown using electron cyclotron resonance chemical vapor deposition".

3. Yue G. Z., Q. Qiu, Bo Gao Y. Cheng, J. Zhang, H. Shimoda, S. Chang, J. P. Lu and O. Zhou, Appl. Phys. Lett., 81, (2002), 355-357, "Generation of continuous and pulsed diagnostic imaging x-ray radiation using a carbon-nanotube-based field-emission cathode".

Z

1. Zhong G., T. Iwasaki, K. Honda, Y. Furukawa, I. Ohdomari, and H. Kawarada, Jpn. J. Appl. Phys. 44, (2005), 1558-1561, "Low Temperature Synthesis of Extremely Dense and Vertically Aligned Single-Walled Carbon Nanotubes".

2. Zhou Dan and Su Wang, Appl. Phys. Lett., 65, (1994), 1593-1595, "Single-walled carbon nanotubes growing radially from YC_2 particles".

Vita

🌀 基本資料

🔹 姓名：洪蔡豪 (Tsai-Hau Hong)

🔹 性別：男

🔹 出生年月日：民國 71 年 6 月 26 日

🔹 籍貫：台灣省新竹市

🔹 通訊地址：新竹市北區竹光路 184 巷 33 弄 13 號

🔹 聯絡電話：(03)5731950

🔹 電子信箱：jef.mse89@nctu.edu.tw

🌀 學歷

🔹 國立交通大學　材料科學與工程研究所

　　(民國 93 年 7 月 至 民國 95 年 7 月)

🔹 國立交通大學　材料科學與工程學系

　　(民國 89 年 9 月 至 民國 93 年 7 月)

🌀 經歷

🔹 國立交通大學材料科學與工程研究所-高等物理冶金助教

　　(民國 93 年 9 月 至 民國 94 年 1 月)(民國 94 年 9 月 至 民國 95 年 1 月)

🔹 國立交通大學工學院專班-奈米結構材料及其製程技術課程助教

　　(民國 94 年 2 月 至 民國 94 年 6 月)

🔹 國立交通大學奈米科技研究所-材料科學與奈米技術課程助教

　　(民國 94 年 9 月 至 民國 95 年 1 月)

🌀 專長

🔹 奈米材料製程與結構分析

🔹 單壁奈米碳管低溫製程與應用